Viscosity, Granular-Temperature and Stress Calculations
For Shearing Assemblies of Inelastic, Frictional Disks

Otis R. Walton
Robert L. Braun

June 25, 1985

Lawrence
Livermore
National
Laboratory

DISCLAIMER

Viscosity, Granular-Temperature, and Stress Calculations for Shearing Assemblies of Inelastic, Frictional Disks[*]

OTIS R. WALTON and ROBERT L. BRAUN
Lawrence Livermore National Laboratory, Livermore, CA 94550

Synopsis

Employing non-equilibrium molecular-dynamics methods the effects of two energy loss mechanisms on viscosity, stress, and granular-temperature in assemblies of nearly rigid, inelastic, frictional disks undergoing steady-state shearing are calculated. Energy introduced into the system through forced shearing is dissipated by inelastic normal forces or through frictional sliding during collisions resulting in a natural steady-state kinetic energy density (granular-temperature) that depends on the density and shear rate of the assembly and on the friction and inelasticity properties of the disks. The calculations show that both the mean deviatoric particle velocity and the effective viscosity of a system of particles with fixed friction and restitution coefficients increase almost linearly with strain rate. Particles with a velocity-dependent coefficient of restitution show a less rapid increase in both deviatoric velocity and viscosity as strain rate increases. Particles with highly dissipative interactions result in anisotropic pressure and velocity distributions in the assembly, particularly at low densities. At very high densities the pressure also becomes anisotropic due to high contact forces perpendicular to the shearing direction. The mean rotational velocity of the frictional disks is nearly equal to one-half the shear rate. The calculated ratio of shear stress to normal stress varies significantly with density while the ratio of shear stress to total pressure shows much less variation. The inclusion of surface friction (and thus particle rotation) decreases shear stress at low density but increases shear stress under steady shearing at higher densities.

INTRODUCTION

The mechanical behavior of cohesionless granular solids is important in a wide variety of industrial, engineering, and scientific fields including such diverse areas as the flow of solids through chemical processing plants, landslides, agriculture, mining, transportation and handling of solids and even recently proposed solar and fusion energy facilities. Despite wide interest and more than 100 years of experimental and theoretical

---

investigations many aspects of the behavior of flowing granular solids are still not well understood. This situation exists primarily because of the difficulties involved in measuring pertinent parameters in such flows. Recent theories based on microstructural considerations[1-5] are providing insight into the differences between the statistical mechanics of systems of dissipative particles and traditional gas-dynamics behavior. This theoretical activity is complemented by recent molecular-dynamics-like computer simulations of shearing flows of inelastic particles[6-9].

The theoretical descriptions have generally dealt with systems of smooth spheres and only very recently have the effects of friction and particle rotation been examined[3]. The shearing flow computer studies, like the work reported in this paper, have generally been limited to two-dimensional systems of disks. Cundall[10] has examined three-dimensional systems of spheres, but only under conditions of quasi-static deformations.

In this work we numerically integrate the equations of motions for all particles in a system undergoing uniform shearing with periodic-boundaries; a configuration patterned after non-equilibrium molecular-dynamics studies of transport coefficients by Hoover[11], Hoover and Ashurst[12] and Evans[13,14]. This simulation differs is some significant ways from the molecular dynamics studies it is patterned after. First and most importantly the particle interactions are non-conservative so that kinetic energy is dissipated in every collision. No artificial "thermostat" or constrained equations-of-motion are needed to maintain a constant temperature under steady shearing conditions. Instead, a natural "granular temperature" or mean deviatoric velocity is determined by the natural progression of dissipative collisions and becomes one of the many output diagnostic quantities calculated. A second distinction is that even though the particles modeled

are symmetric circular disks, they experience tangential (non-central) friction forces during collisions. These friction forces result in particle rotations and also contribute non-symmetric terms to the stress tensor. While a non-symmetric stress tensor could result from such forces, in all uniform shearing flows calculated a symmetric stress tensor was obtained except for time averages over very short time periods (including only a few collisions). It should be noted, however, that in many cases the conditions modeled are far from a traditional thermodynamic equilibrium state, as evidenced by the anisotropy in both the pressure and velocity distributions. This anisotropy was especially apparent at low solids concentrations with highly dissipative particles.

UNIFORM SHEAR MODEL

The two-dimensional steady-state shearing model consists of an assembly of a small number of equal-sized circular disks (usually 30) in a rectangular calculational cell with periodic boundaries on all four sides. The image cells above and below the primary cell move to the right and left, respectively, creating a layered shearing structure. Figure 1 shows the primary calculational cell and the nearest moving periodic image cells, with one particle and its various periodic images. The initial coordinates of the particles are automatically generated by placing a specified number of particles in a hexagonal, close-packed array then increasing the interparticle separation to uniformly fill the cell. The particles' radii are set to unity and the cell dimensions selected such that a specified solids packing fraction is obtained for the given number of particles. Initial particle velocities are randomly assigned to one-half of the particles and velocities in the opposite directions are assigned to the remaining particles in order to obtain
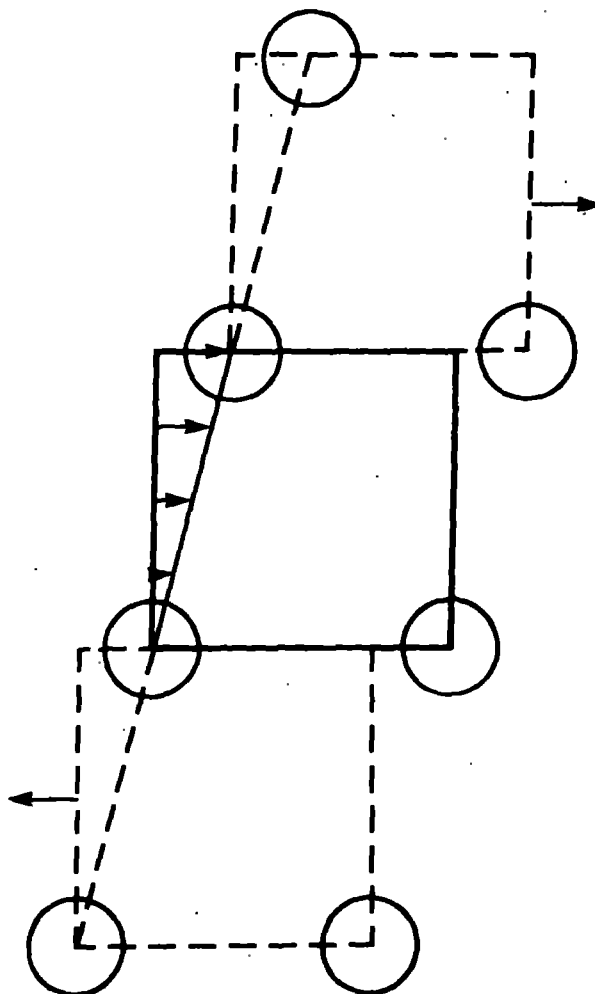
Figure 1. One particle and its periodic images in the primary calculational cell and in the nearest moving periodic image cells used to produce steady state shearing.

zero velocity for the system center of mass (without shearing). All velocities are initially scaled to achieve an estimated average deviatoric particle velocity. Then an additional steady-state shearing velocity, proportional to the y-coordinate, is superimposed in the x-direction. Newton's equations-of-motion for particle translation and rotation are solved by an explicit, time-centered, finite-difference algorithm (with an iterative predictor-corrector algorithm employed when velocity-dependent forces are used). Particle interactions are calculated for the collision of each

original particle with every other particle or with the nearest periodic image of every other particle in the infinite lattice of image cells. The moving image cells provide a steady source of kinetic energy to the system which is dissipated by the frictional, inelastic collisions between particles. For each point calculated in the parameter study below, the system was allowed to arrive at steady state (usually taking from 20 to 100 collisions per particle) and then cumulative time averages were taken of various quantities for a period typically including from 200 to 1500 collisions per particle. After each calculation a running average graph of each time-averaged quantity was made for ease of evaluating whether steady state had been achieved during the averaging time period. Each particle's deviatoric velocity was obtained by subtracting the mean shearing field $u_x = \dot{\epsilon} \, y$ from the calculated particle velocity. In addition, the following quantities were monitored during each calculation: the mean translational kinetic energy density in the system, $\langle KE_T \rangle / A$, where

$$\langle KE_T \rangle = \langle \sum_i \frac{1}{2} m_i \left[(v_{xi} - u_x)^2 + v_{yi}^2 \right] \rangle ,$$

the average deviatoric speed of the particles, $\langle \upsilon^2 \rangle^{1/2}$, where

$$\langle \upsilon^2 \rangle^{1/2} = \langle \frac{1}{n} \sum_i \left[(v_{xi} - u_x)^2 + v_{yi}^2 \right] \rangle^{1/2} ,$$

the average rotational kinetic energy density, $\langle KE_r \rangle / A$, where

$$\langle KE_r \rangle = \langle \sum_i \frac{1}{2} I_0 \, \omega_i^2 \rangle ,$$

the mean rotational velocity of the particles, $\langle \underline{\omega} \rangle$, and the time average of the momentum-flux-density tensor (i.e., the stress tensor) instantaneously given by the expression

$$\underline{\underline{P}} = \sum_i (\underline{v}_i - \underline{u})(\underline{v}_i - \underline{u}) + \sum_{j > i} \underline{R}_{ij} \underline{F}_{ij}$$

in which the first term on the right is a symmetric dyad representing the

kinetic contribution to the stress and the second dyadic term represents the collisional or potential contribution to the stress tensor and contains antisymmetric components if the force between two particles, $\underline{F}_{ij}$, is not parallel to the line joining their centers, $\underline{R}_{ij}$. The kinetic and collisional terms for the stress tensor were separately averaged in time and a number of quantities involving the stress tensor were also calculated including: the effective viscosity, $\eta = -(p_{xy} + p_{yx})/2\dot{\varepsilon}$, where $\dot{\varepsilon}$ is the shear rate, $(\partial u_x/\partial y)$; the effective compressibility of the system, $A(p_{xx} + p_{yy})/2<KE_T>$, and various ratios of components of the stress tensor.

Interparticulate Normal Force Model

During each interparticle collision the actual normal and tangential forces acting between real macroscopic disks are approximated by force displacement models that include position-dependent hysteresis. Approximately 50 calculational time steps are used to calculate a typical collision so that the accuracy of the trajectories and energy losses occurring during each collision is on the order of one part in 10^4. The details of the calculations leading to the model for the inelastic, frictional contact forces used in this study are reported elsewhere[15] so they are only briefly reviewed here. Dynamic finite element calculations using the DYNA2D computer program[16] confirm that little residual energy remains in elastic waves within two perfectly elastic spheres after a direct impact. These calculations also show that contact time during normal impacts varies as the inverse one-fifth power of the relative approach velocity -- as predicted by Hertzian contact theory for impacts between perfectly elastic spheres[17]. These calculations confirm that, in general, collisions between elastic spherical particles can be closely approximated by assuming that a non-linear

(Hertzian contact) spring acts between two essentially rigid bodies. Further finite element calculations using elastic-perfectly-plastic material models show that the coefficient of restitution for normal impacts is a strong function of the impact velocity, in agreement with experimental evidence[18]. Further quasi-static finite-element calculations using the NIKE2D computer program[19] reproduced Hertz's 3/2-power normal force variation with relative approach for perfectly elastic spheres. An elastic-perfectly-plastic material description in the same finite element calculations resulted in an almost linear relationship between normal force and initial loading displacement. Experimental measurements of load vs. relative approach for steel ball bearings striking the flat end of an aluminum rod also show an almost linear loading after a small initial curved region[18]. Both the finite element calculations of elastic-plastic spheres and the tests of steel balls on aluminum exhibited very steep unloading curves that were almost linear. The slopes of these unloading lines were steeper for impacts that experienced a larger maximum force before unloading (i.e., with higher velocities of impact).

For ease of calculation in our two-dimensional disk interaction model we approximate the behavior obtained in the above calculations (and observed in the experiments) with a partially-latching-spring model. In this model, the normal force is given by

$$N = K_1 \alpha \qquad \text{for loading, and}$$
$$N = K_2(\alpha - \alpha_0) \qquad \text{for unloading,} \qquad (2)$$

where α is the relative approach (overlap) after initial contact, and α_0 is the value of α where the unloading curve goes to zero. No negative (or tensile) values are allowed for N. Figure 2 shows a schematic of this partially-latching-spring force model. Initial loading is along the line from point a to point b with slope K_1. If unloading is initiated after reaching point b then it will be along the line from b to c. Reloading from point c
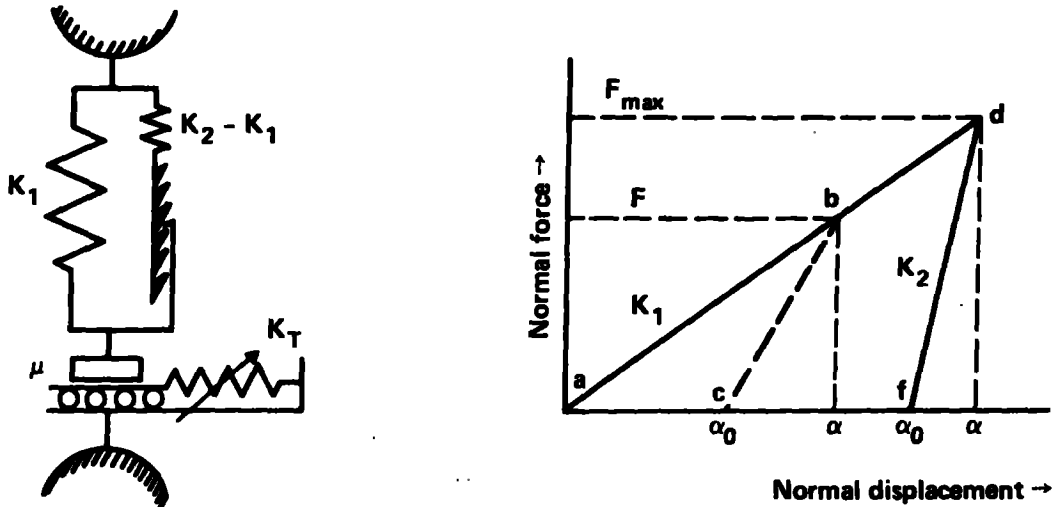
$$e = \sqrt{\frac{K_1}{K_2}}$$

Variable latching spring:

$$K_2 = K_1 + S\,F_{max}$$

Figure 2. Schematic of partially-latching-spring model and the corresponding force deflection curve used to describe inelastic normal direction forces acting between two colliding disks.

follows the path c, b, d and subsequent unloading from point d follows the path d, f, c, a. The normal force model thus exhibits a position dependent hysterisis which results in a less-than-unity coefficient of restitution for normal impacts. The model is employed in two modes. In the constant coefficient of restitution mode all unloading lines (e.g. $\overline{b\,c}$ and $\overline{d\,f}$) have exactly the same slope, K_2, and the resulting coefficient of restitution, e, is given by.

$$e = (K_1/K_2)^{1/2} \tag{3}$$

where -e is the ratio of initial to final relative velocities in the normal direction. In the variable coefficient of restitution mode, the unloading slope, K_2, is a linear function of the maximum force achieved before

unloading,

$$K_2 = K_1 + SF_{max}. \tag{4}$$

Using this model, the coefficient of restitution depends on the relative

velocity of approach, v_o, as given by

$$e = [\omega_0/(Sv_0 + \omega_0)]^{1/2} \tag{5}$$

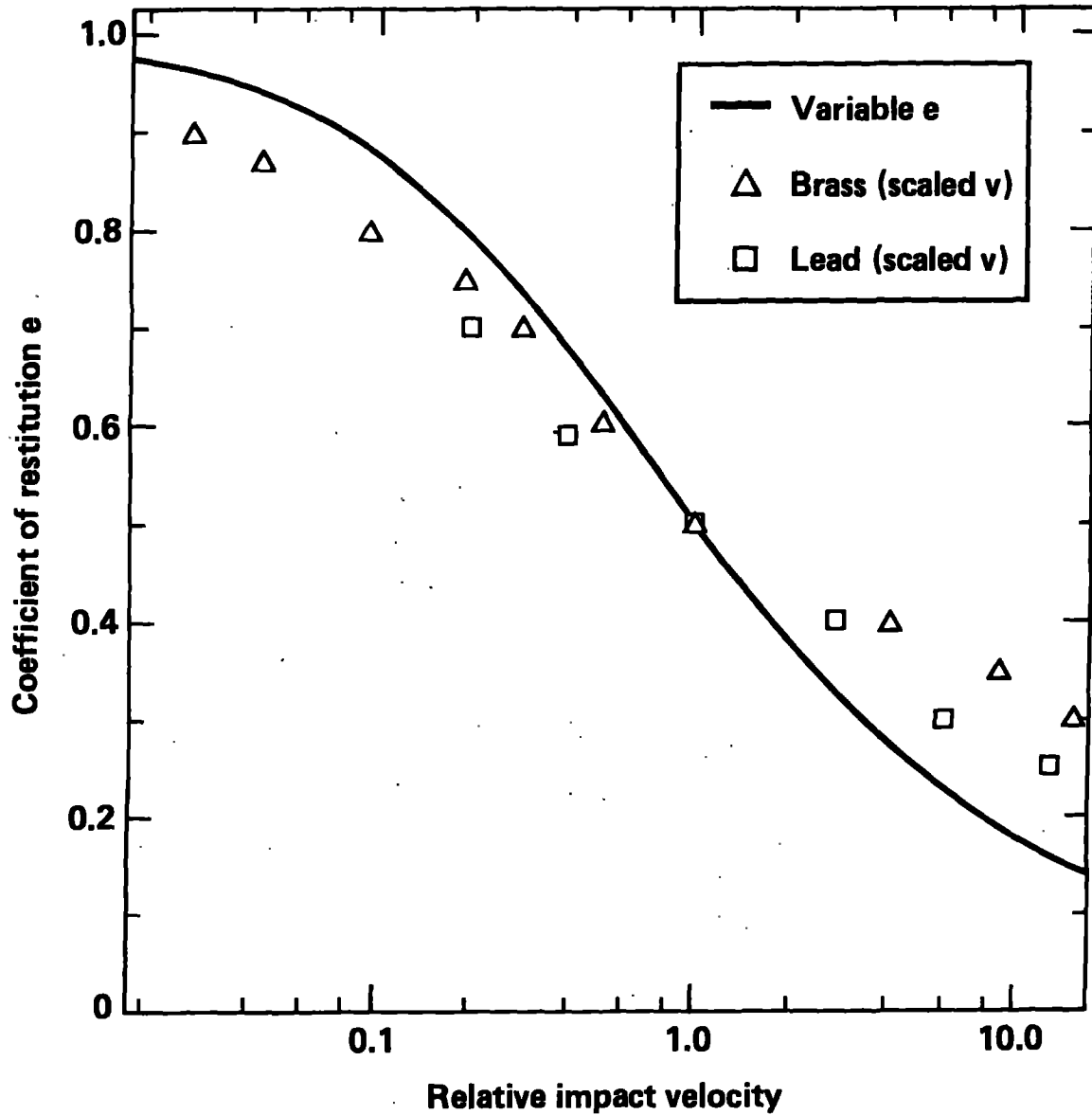where $\omega_0 = (2K_1/m)^{1/2}$. Figure 3 shows this variation of e with

Figure 3. Coefficient of restitution given by variable e model (Equations 2 to 5) and obtained in impact tests with identical spheres of brass and lead[18]. Velocities scaled so that 1 corresponds to e = 1/2.

non-dimensional impact velocity, $v_0/v_{0.5}$ (where $v_{0.5}$ is the relative approach velocity that produces a coefficient of restitution of one-half). Also shown in Figure 3 are values of the coefficient of restitution for collisions between identical spheres of brass and lead as reported by Goldsmith[18]. As can be seen from this figure the variable coefficient of restitution model of equations (4) and (5), while not a perfect fit, matches the experimental data much closer than would a constant coefficient of restitution. Because of the simplicity of the form of equation (4) we choose to use this model for the variable coefficient of restitution calculations in the parameter study below. It is expected to give a difference from constant e behavior that is at least as large as might be expected for real materials.

Incrementally Slipping Friction Model

The tangential friction force model used in these calculations is patterned after theoretical models for the friction forces acting between elastic spheres in contact developed by Mindlin[20] and Mindlin and Deresiewicz[21]. Mindlin's expression for the tangential compliance acting during small displacements is based on the assumption that the approximate Hertzian normal stress distribution over the circular area of contact is unaffected by the tangential displacement. In this theory, the effective tangential stiffness of a contact decreases with tangential displacement until it is effectively zero when full sliding occurs. We employed functions that approximate the expressions of Mindlin and Deresiewicz. The effective tangential stiffness, K_T, used in the model contacts is given by

$$K_T = \begin{cases} K_0 \left(1 - \dfrac{T-T^*}{\mu N - T^*}\right)^\gamma & \text{for slip in one direction (T increasing)} \\[4mm] K_0 \left(1 - \dfrac{T^*-T}{\mu N + T^*}\right)^\gamma & \text{for slip in the other direction (T decreasing)} \end{cases} \tag{6}$$

where T is the total tangential force, K_0 is the initial tangential stiffness, μ is the coefficient of friction, N is the total normal force, γ is a fixed parameter usually set to one-third to agree with Mindlin's theory, and T^*, which is initially zero, is subsequently set to the value of the total tangential force, T, whenever the relative tangential slip reverses direction. If the normal force, N, changes during the contact, the value of T^* in the above expressions is scaled in proportion to the change in normal force.

On each explicit time step of the finite difference calculations a new tangential force, T', is calculated incrementally from the old value of the tangential force, T, the effective tangential stiffness, K_T, and the amount of relative surface displacement between the contacting particles, Δs, by the expression

$$T' = T + K_T \Delta s \qquad\qquad (7)$$

with K_T given by equation (6). Thus, in order to calculate the total tangential force acting between each pair of particles, we need to keep only two quantities, T and T^* from one time step to the next.

Figure 4 shows the tangential force vs. tangential displacement as generated by equations (6) and (7) for a series of ever increasing amplitude oscillations of the relative tangential surface displacement, s, with a constant normal force, and an exponent $\gamma = 1/3$. Experimental measurements of initial displacements of frictional forces acting between metals in contact (non-spherical bodies) produce force deflection curves that are qualitatively quite similar to the model curve of Figure 4, but with a more gradual change in slope, as would be produced with a larger value for the exponent, γ, in the model (for example, see Oden and Martins[22]).
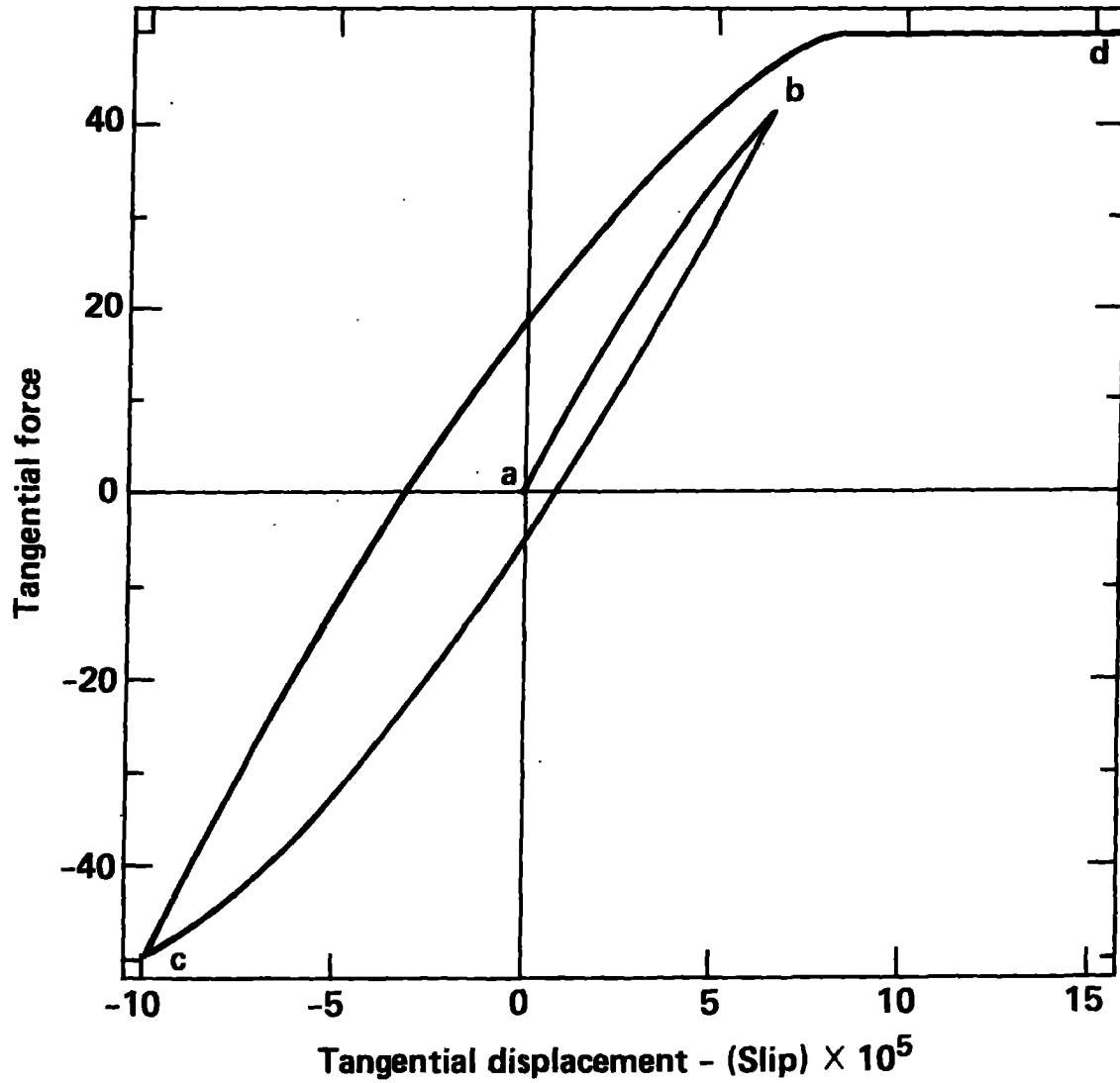
Figure 4. Tangential force generated by incrementally-slipping friction model
with a constant normal force and ever increasing amplitude
alternating tangential displacements (γ=1/3 in Equation 6).

For comparison with rigid body models that include frictional transfer of
tangential impulse in instantaneous collisions we can examine the effective
coefficient of rotational restitution, β, defined by

$$v'_s = -\beta v_s$$

where v_s is the relative tangential surface velocity between the two
particles just before impact and v'_s is that relative velocity immediately
after the particles came apart. The value of β ranges from -1 for smooth

(frictionless) particles to +1 for perfectly rough, perfectly elastic particles. During a frictional encounter the tangential impulse that can be transferred from one particle to the other is limited by the friction coefficient and the normal impulse transmitted, so that,

(tangential impulse) $\leq \mu$ (normal impulse).

Thus, for two identical particles the maximum change in the relative center of mass velocity in the direction tangent to the contact, $(\Delta v_t)_{max}$, is given by

$$(\Delta v_t)_{max} = - sign(v_s)\mu(1+e)v_n/2$$

where v_n is their relative normal direction velocity, and v_s is their relative tangential surface velocity just before contact. By requiring that the angular momentum about the contact point be conserved we find an upper limit expression for β,

$$\beta \leq -1 + \mu(1+e)|v_n/v_s|(1+mr^2/I_0) \qquad (8)$$

for collisions between equal sized particles, where mr^2/I_0 is 2 or 5/2 for disks or spheres, respectively. This expression results in values of β that can exceed one when v_s is near zero (since the expression is singular at that point). Various extra assumptions are often employed to restrict β to values less than zero (e.g. assuming that friction can only reduce the relative surface velocity and could not increase it once a value of zero is reached[16]) or to values less than one to conserve energy[*].

The tangential and normal force models employed in this study automatically produce values of β that are always at or below the theoretical friction limit of equation (8). These models also include the possible effect of spring-back of shear-deformation on the surface and can produce values of β that are greater than zero for many impact situations with relatively small initial relative tangential velocities. Figure 5 shows the frictional upper bound to the tangential restitution coefficient, β,
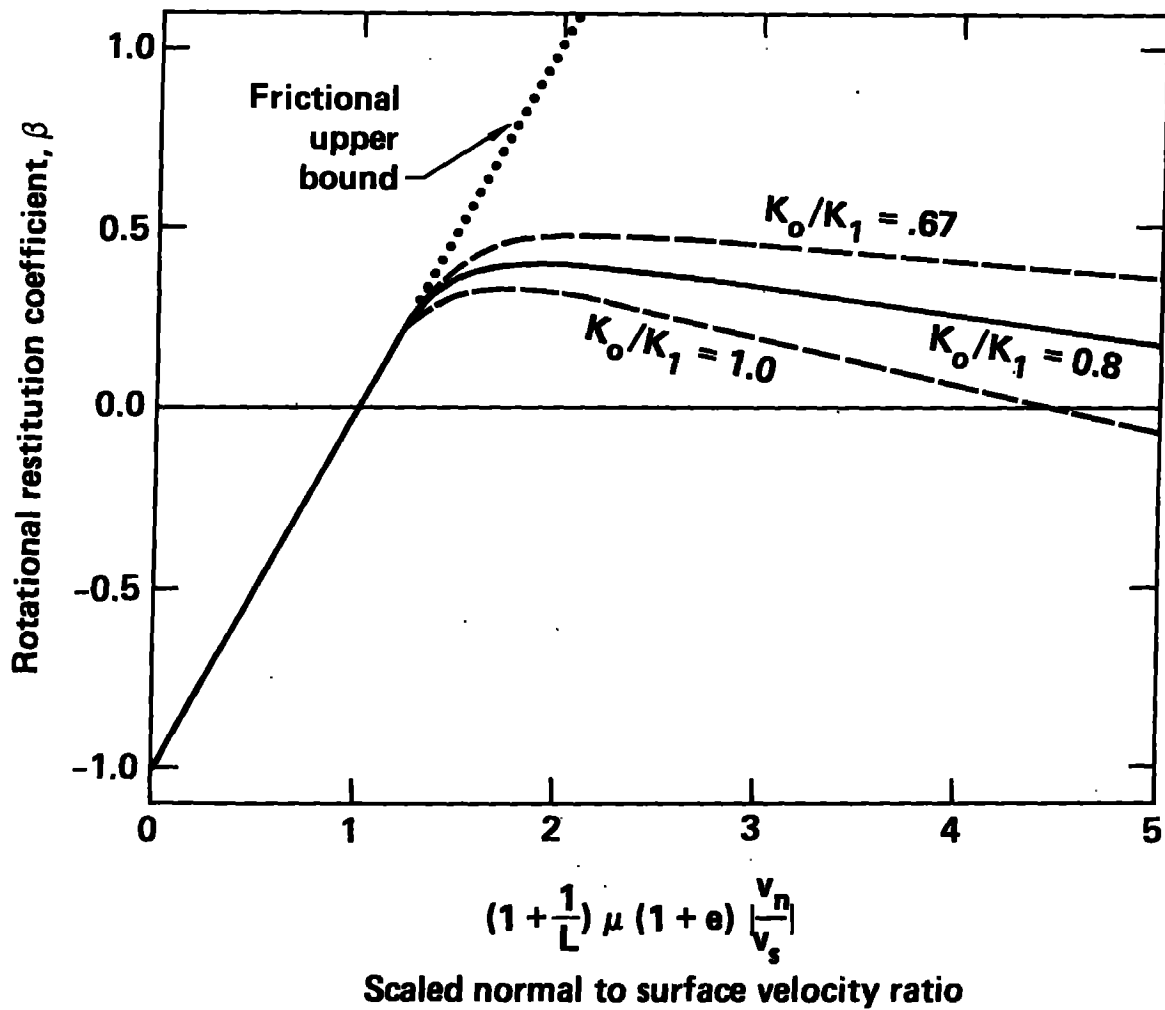
Figure 5. Rotational restitution coefficient, β, as a function of scaled ratio of normal to tangential surface velocities for impacting spheres. Curves are for various ratios of initial tangential to normal stiffness, dotted line is frictional upper bound, Equation (8). (L = $\frac{1}{2}$ for disks and 2/5 for spheres).

(dotted line) and the dependence of β as calculated by the above tangential and normal force models for collisions between two equal-sized spheres with various initial relative tangential-to-normal velocity ratios. The left-hand side of the horizontal axis in this figure corresponds to a glancing impact and the right-hand side to an incident angle about 30° from normal incidence for non-rotating particles with friction and restitution coefficients of 0.5 and 0.8, respectively. For comparison, the theoretical work of Lun and

-14-

Savage[4] uses various constant values of β (between -1 and 1) independent of initial velocity ratio. Campbell and Gong[6] use a single value of β = 0.0, corresponding to near infinite friction, for all collisions between rough circular particles. The exact shape of the deviation from the frictional upper bound curve calculated by the present models depends on the ratio of the initial shear to normal stiffness. The three curves in Figure 5 represent three possible values for this ratio of 1.0, 0.8, and 0.67. The upper and lower (dashed) curves represent the upper and lower theoretical limits given by Mindlin corresponding to elastic spheres with the Poisson's ratios of 0.0 and 0.5, respectively. The middle curve corresponds to a realistic initial tangential stiffness to normal stiffness ratio of 0.8 which was used for all calculations in the parameter study below. Most of the calculated quantities in this study are not extremely sensitive to the exact form of the rotational coupling. This is evidenced by the relatively good agreement obtained between the stresses calculated in this study and the results of Campbell and Gong[6] using a constant β = 0.0 rotational coupling.

RESULTS

Comparison with 2-D molecular dynamics

To test the accuracy of the model's integration scheme and the validity of the periodic-image collision calculations, we compared our compressibility factor with that calculated by Hoover and Alder for a 12-particle system of rigid disks having a solids packing fraction 20% less than that for hexagonal close packing[23]. For this comparison, we set the coefficient of restitution to unity, the shear rate and the friction coefficient to zero and obtained a thermodynamic equilibrium value for the compressibility of a 12-particle system using interparticulate stiffnesses of $K_1 = 10^6$ and 10^7 (with unit radius and unit mass disks). The calculated compressibility was corrected for

the increased number of collisions occurring in a system with a fixed center of mass (after Hoover and Alder[23]), then plotted against the inverse of the particle stiffness and extrapolated to zero inverse stiffness (corresponding to perfectly rigid particles). The extrapolated value of 7.43 was in almost exact agreement with the value of 7.42 reported by Hoover and Alder. In a further comparison with these rigid disk results we calculated the effective compressibility for a system of 30 smooth (frictionless) particles in a series of non-equilibrium steady-state-shearing configurations ranging in solids concentration from 0.025 to 0.775, with a coefficient of restitution, e = 0.80. Each individual solids packing fraction had a unique mean deviatoric velocity (and thus a unique kinetic energy density); however, this mean deviatoric velocity changed by over an order-of-magnitude as the solids packing fraction changed at the fixed shear rate. Also, the ratio of stress components p_{xx}/p_{yy} varied from 1.4 to 0.8 over the calculated range of densities, yet the effective compressibility for this non-equilibrium system was surprisingly close to the compressibilities calculated in the equilibrium rigid-disk study of Hoover and Alder. Figure 6 shows the compressibility results of Hoover and Alder for their system of 12 particles (without an explicit first order phase change) and also for their system of 72 particles exhibiting a first order phase change from fluid to solid between the solids fractions of $v = 0.665$ and $v = 0.705$. The present frictionless non-equilibrium shearing results shown on that same figure, are extremely close to Hoover and Alder's rigid disk results up to the phase change density. Beyond that density they appear to be an extension of the fluid-like behavior, at least up to solids concentrations of $v = 0.700$. Examination of computer generated motion pictures of the particle motions in these shearing calculations verified that fluid-like behavior was indeed being obtained up to solids frictions as high as $v = 0.775$.
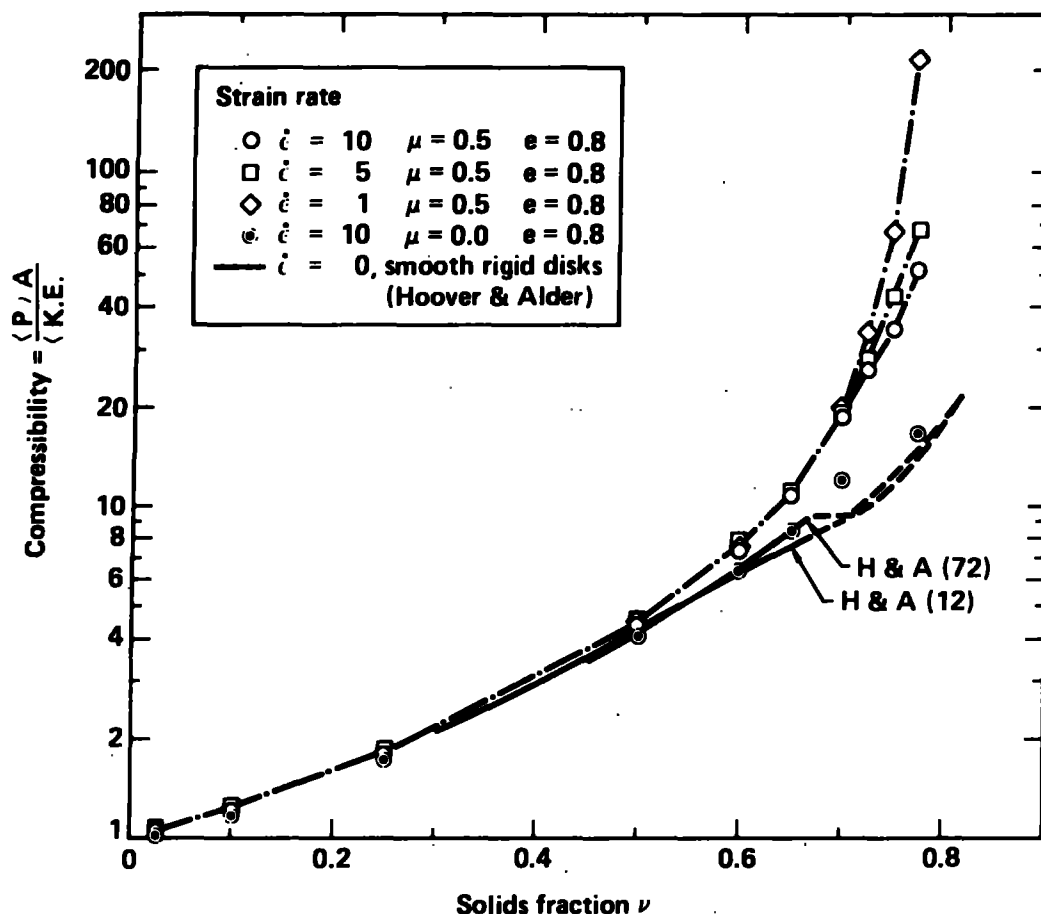
Compressibility = $\frac{\langle P \rangle A}{\langle K.E. \rangle}$

Solids fraction ν

Strain rate

O $\dot{c}$ = 10 μ = 0.5   e = 0.8
□ $\dot{c}$ = 5 μ = 0.5   e = 0.8
◇ $\dot{c}$ = 1 μ = 0.5   e = 0.8
⊚ $\dot{c}$ = 10 μ = 0.0   e = 0.8
—— $\dot{c}$ = 0, smooth rigid disks
        (Hoover & Alder)

H & A (72)
H & A (12)

Figure 6.   Two-dimensional compressibility as calculated for 12 or 72 smooth rigid disks in thermodynamic equilibrium by Hoover and Alder[23] and as calculated in the present non-equilibrium shearing flow study with 30 inelastic, frictionless (lower points) and frictional (upper curves) disks at various shear rates.

Also shown on Figure 6 is the effective compressibility calculated for a 30-particle system of frictional disks with a friction coefficient of μ = 0.50, at three different shearing rates. These three curves lie essentially on top of one another (and significantly above the frictionless particle curves) until a packing fraction of 0.700 is reached at which point they diverge with the lowest shear rate producing the highest effective compressibility. This lowest shear rate curve has the lowest kinetic energy density and, at the high solids packing fractions, includes many continuous sliding and rolling contacts. This behavior deviates most significantly, from

the thermodynamic equilibrium smooth rigid disk behavior. All compressibility curves on Figure 6 approach unity as the solids fraction goes to zero -- corresponding to near ideal-gas-like behavior.

To test the accuracy of our steady-state shear calculations, we compared our calculated viscosity with that calculated by Evans[24] for a non-equilibrium molecular dynamics system of soft disks interacting with an inverse 12th-power potential. We modified our model to use the same inverse 12th-power interaction potential. A 30-particle system was sheared at a strain rate corresponding to Evans' reduced strain rate of 0.248. The average deviatoric velocity was constrained to its initial value for the entire calculation using Hoover's constrained equation-of-motion technique[11]. The time-averaged reduced viscosity calculated for this system was approximately 2.5% higher than Evans' value of 2.835. A number of factors may have contributed to this slight discrepancy: the use of a 30-particle system instead of the 32-particle system used by Evans, the use of a cumulative average that included some non steady-state results early in the calculation, and the use of a perfectly square calculational cell (the aspect ratio of Evans' calculational cell is not known). In view of these considerations we judged that our model was functioning essentially as intended.

Steady-State Shearing Results

A parameter study was conducted to examine the effects of shear rate, solids packing, friction, and elasticity on various rheologic properties of an assembly of particles in steady shear. A representative two-dimensional granular material consisting of 30 identical disks, each with unit mass and unit radius, and an interparticulate normal stiffness of 1×10^6 and an initial tangential stiffness of 0.8×10^6 was used for this study. The shear rate was varied from 1 to 10 inverse time units and the fraction of the

cell area covered by particles (i.e., the solids fraction) was varied from 0.025 to 0.825. The friction coefficient was set at 0.5 for most calculations; however, calculations were also done with $\mu = 0.0$ to observe the sensitivity of the results to the inclusion of particle rotation. Fixed coefficients of restitution of 0.6, 0.8, and 1.0 were examined along with a representative variable coefficient of restitution material (with S = 73 in equations 4 and 5). The middle (solid) curve on Figure 5 gives the rotational coupling for the nominal material parameters with $\mu = 0.5$ and e = 0.80. An explicit calculational time step of 4.44×10^{-5} was used in all calculations. This corresponds to roughly 50 time steps during a typical two particle collision. In addition to the 30-particle results described below, systems with 12 and 56 particles were also examined at a solids concentration of $\nu = 0.700$. The 12-particle system gave considerably higher values for both normal and shear stresses, primarily due to continuous contact arches that temporarily formed across the entire periodic cell height. The resulting, short-duration, high stresses increased the cumulative time averages of the stress components by as much as 30 to 40% above the 30-particle averages. The 56-particle system gave results that were generally within the statistical scatter of the 30-particle results. Thus, we used the 30-particle system as an efficient representative sample for the uniform shearing calculations.

Effective Viscosity, Temperature and Pressure

Bagnold[24] studied neutrally buoyant wax spheres and used simple physical arguments to hypothesize that the stresses in shearing granular assemblies should be proportional to the square of the shear rate. Since Bagnold's arguments apply equally well to two-dimensional systems, we examined the variation of shear stress with shear rate in our periodic cell system.
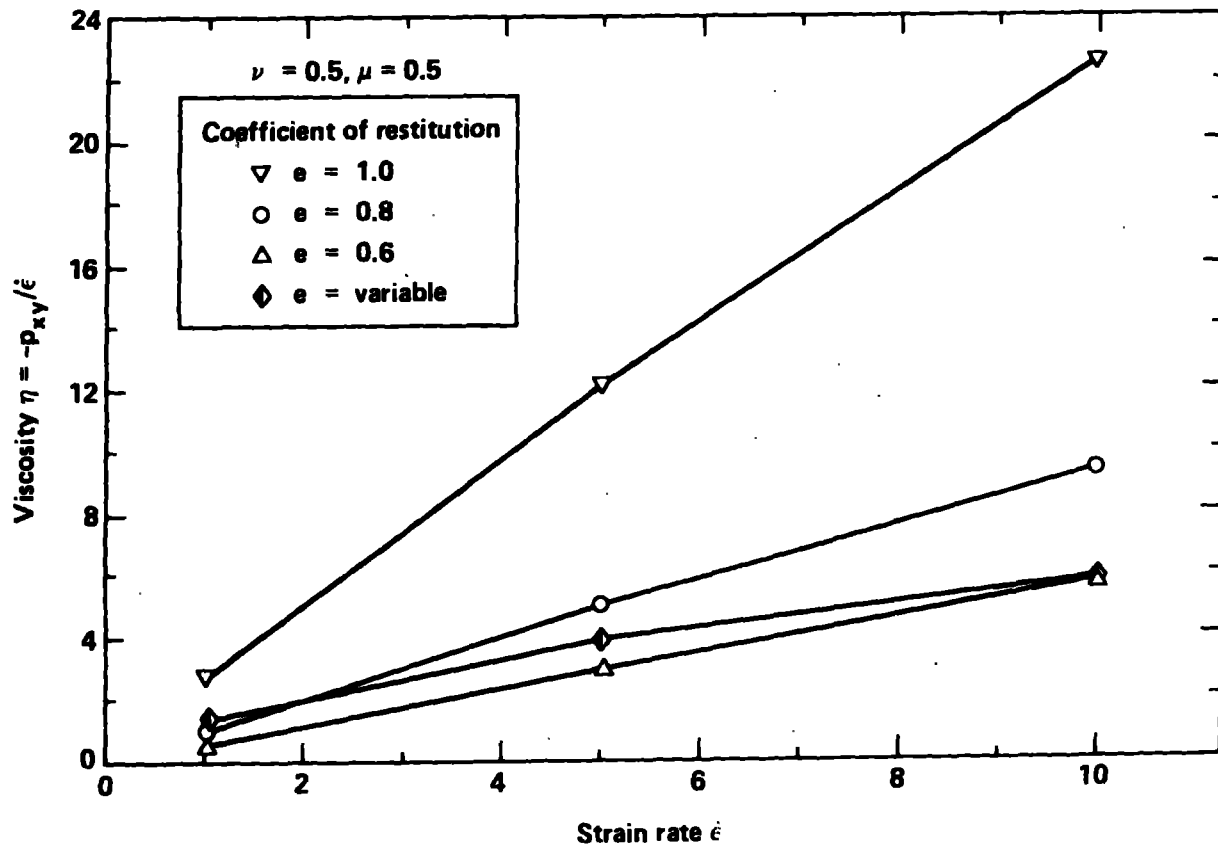
Figure 7.   Effective viscosity as a function of strain rate calculated for a system of 30 disks in steady shear at a solid fraction of $\nu = 0.50$.

Figure 7 shows the effective viscosity calculated for our 30-particle system as a function of strain rate, at a solids packing fraction of $\nu = 0.500$. Bagnold's shear stress variation would produce straight lines passing through the origin on this graph. As can be seen from this figure, our calculated shear stress does increase nearly with the square of the shear rate for particles with a constant coefficient of restitution. However, for disks interacting with the variable coefficient of restitution model of equations (4) and (5), the shear stress increases much less rapidly. We examined this behavior at a number of solids packing fractions and obtained similar
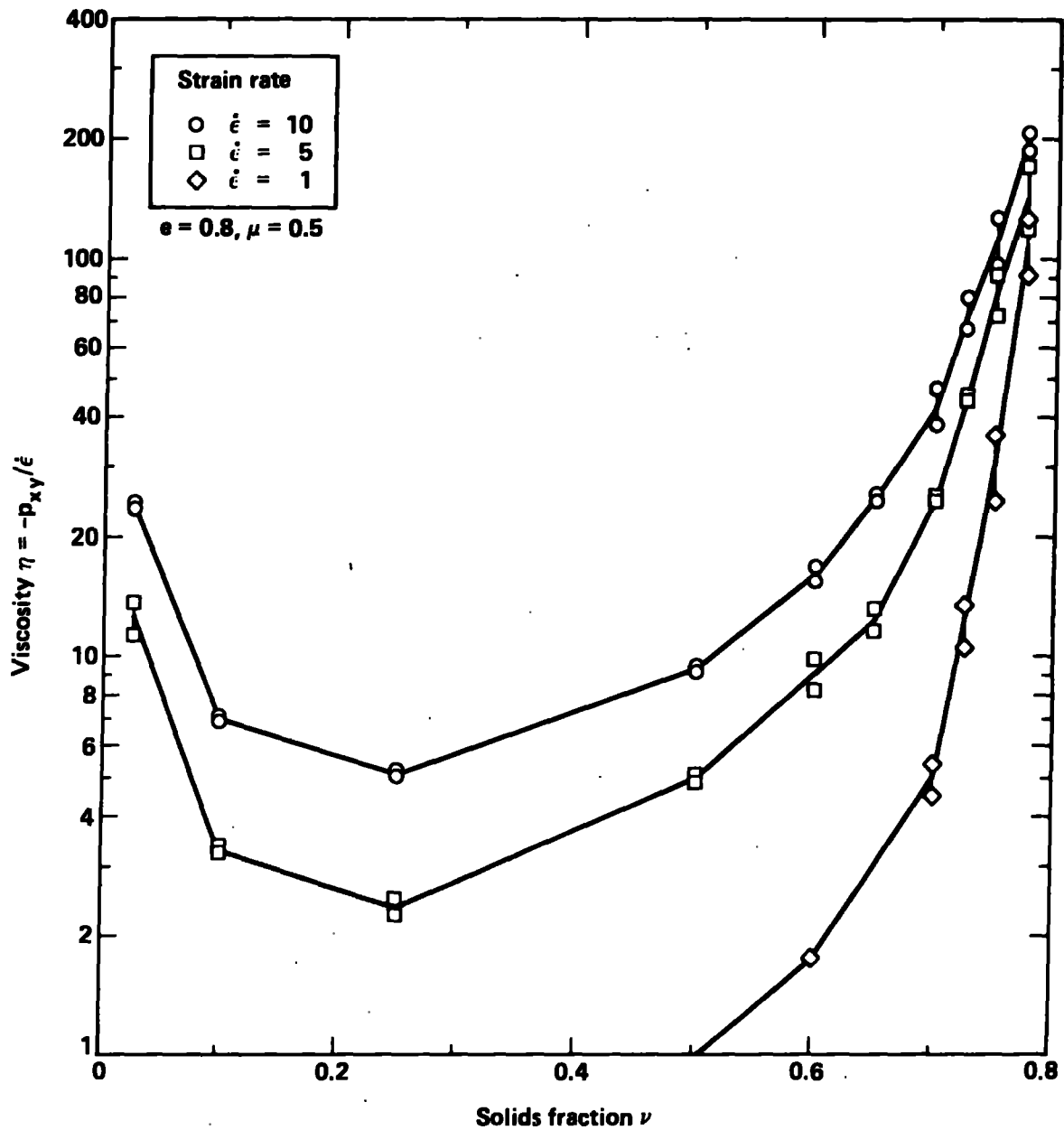
Figure 8. Effective viscosity as a function of solids concentration calculated for 30 inelastic frictional disks in steady shear at various rates.

results. Figure 8 shows the calculated viscosity as a function of solids

packing fraction for various strain rates. The shape of each of these curves

(i.e., high at both low and high solids fractions and passing through a

minimum at a solids fraction near 0.3) is typical of the behavior calculated

for each component of the stress tensor. This behavior is understandable when

we realize that these curves are constant-shear-rate curves, not isotherms. As the solids fraction in the system decreases the cell size increases proportionately. In order to obtain the same mean shear rate the velocity of the moving periodic image cells also increases inversely with the decrease in solids packing. However, at lower particle densities the frequency of collisions decreases more rapidly than simply the inverse of the particle density. Thus, there are fewer dissipative collisions at low density. The net result is a significant increase in the mean deviatoric particle velocities at low solids packing. Figure 9 is a plot of the r.m.s. deviatoric particle velocity (divided by the product of the shear rate and the particle diameter) as a function of solids packing fraction. This dimensionless velocity ratio corresponds to the inverse of the dimensionless velocity ratio, R_s, used by Jenkins and Savage[1] and by Lun et al.[3]. The (solid) central curve on Figure 9 is based on calculations at three different shear rates and shows that the deviatoric particle velocity does indeed scale directly with the shear rate (for particles with a constant coefficient of restitution). Each of the other (dashed) curves on Figure 9 was generated from calculations at just one shear rate ($\dot{\epsilon}$ = 10). However, it is expected that calculations at other shear rates would be essentially the same except for the variable coefficient of restitution (lowest) curve. For the variable coefficient of restitution model, lower shear rates correspond to a lower mean deviatoric velocity, resulting in a higher mean effective coefficient of restitution as the shear rate is reduced. A few calculations were performed at low shear rates with the variable e model and they did indeed lie significantly above the variable e curve of Figure 9, corresponding to a higher mean effective coefficient of restitution. (These points were omitted from the figure to provide better clarity for the fixed e curves).
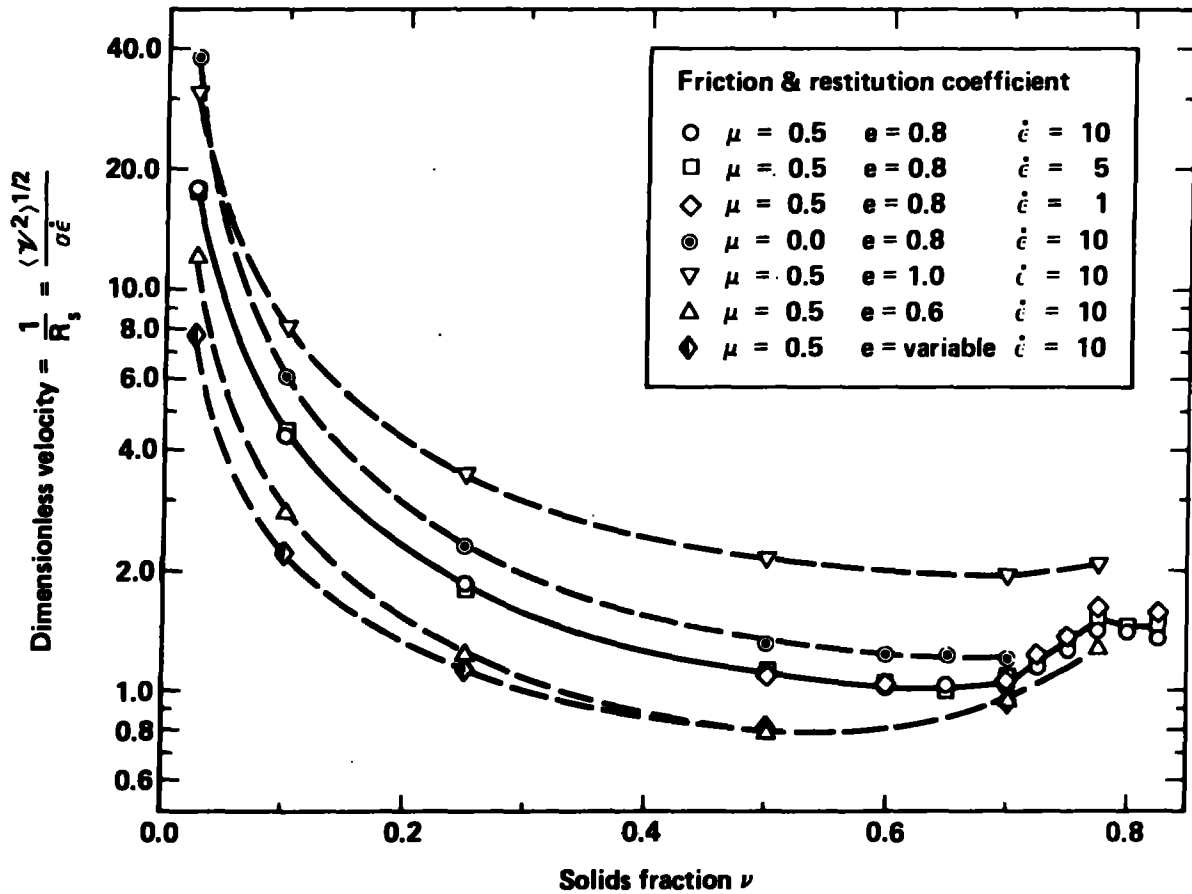
Figure 9. Calculated r.m.s. deviatoric velocity ratio for 30-disk system at
shear rates of 1, 5, and 10 with μ = 0.5 and e = 0.80 (solid
curve) and with other values of e and μ including the variable e
model at a shear rate of 10 (dashed lines).

The substantial increase in mean deviatoric particle velocities and the
large mean free path between collisions at low solids concentrations causes
all components of the stress tensor to be dominated by kinetic contributions
at these densities while at high solids concentrations collisional (or
potential) contributions dominate each component of the stress tensor. Figure
10 shows a representative plot of the total pressure P= $(p_{xx} + p_{yy})/2$ and
the kinetic and collisional components of that pressure as functions of solids
packing fraction. As seen in this figure, the kinetic and potential
components are nearly equal at a packing fraction near ν = 0.30, with the
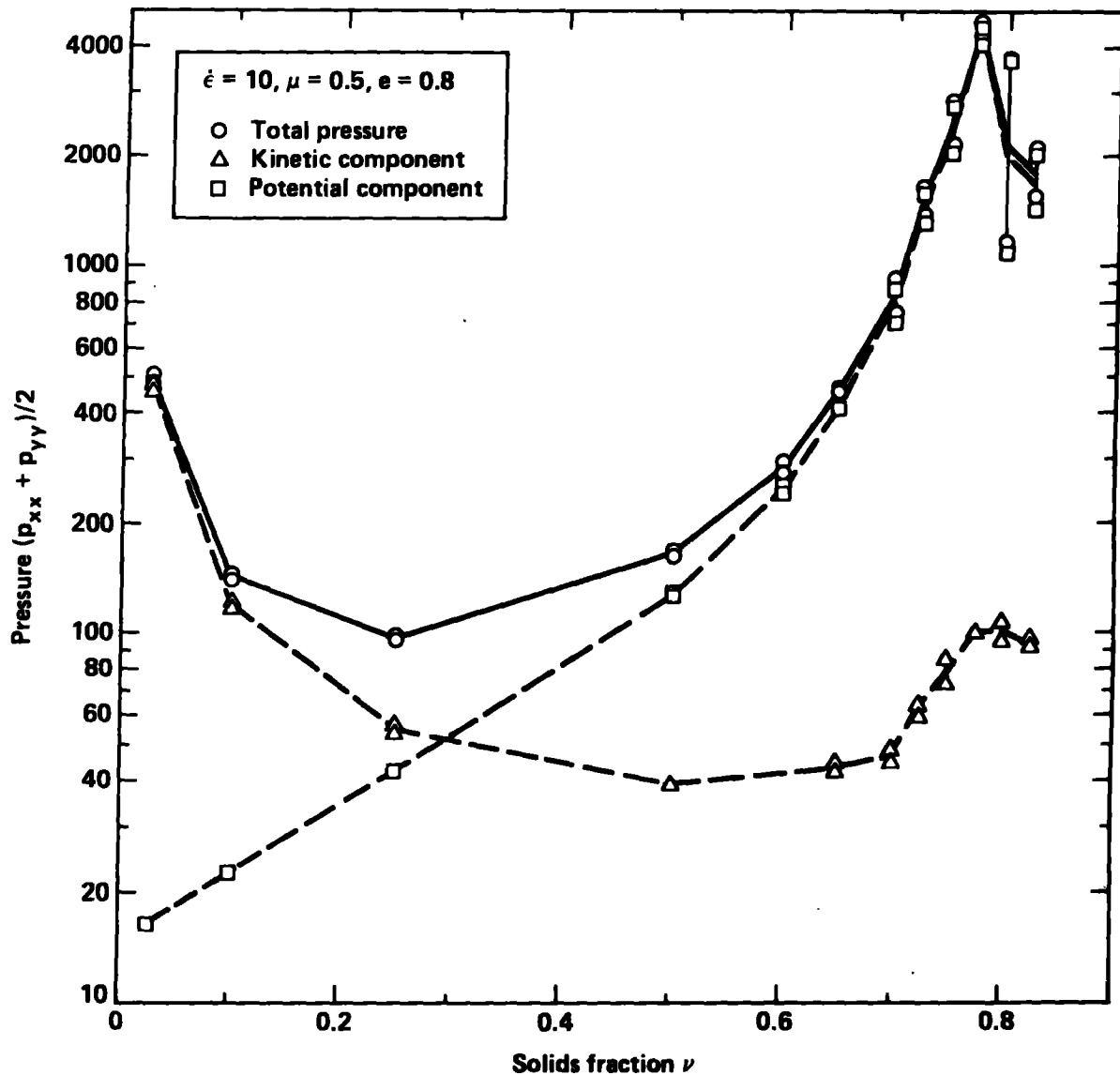kinetic term dominating at all lower solids concentrations and the collisional

Figure 10. Calculated total pressure, kinetic, and collisional components of the pressure for 30 inelastic, friction particles in steady shear flow. Symbols represent time average for each calculation at each condition.

term dominating at all higher densities. This result is consistent with the two-dimensional calculations of Campbell and Gong[6] which also show the kinetic and potential terms having comparable magnitude near ν = 0.3. This result is also in qualitative agreement with the theory of Lun et al.[3] which predicts similar behavior for three-dimensional systems of smooth inelastic

particles. Two-dimensional Monte-Carlo simulations of inelastic frictional disks currently in progress by Hopkins and Shen[26] also agree quantitatively with these results for solid fractions in the range from 0.1 to 0.6.

The abrupt change in slope of the total pressure curve above a solids fraction of 0.775 in the present study occurs because the mode of shearing changes above that density. At densities below ν = 0.775 the shearing is nearly uniform across the calculational cell and "snapshots" of the particle configurations look very much like a two-dimensional fluid. At high densities crystalline regions occupy a large part of the cell with shearing usually occuring in a distinct layer. Figure 11a shows a typical particle position distribution for a solids fraction of ν = 0.650 and Figure 11b shows a typical "snapshot" for a calculation with a solids fraction ν = 0.800. In this figure, the deviatoric velocity and the rotational velocity of each particle are shown as vectors within each particle. At the high density rolling contacts clearly exist and most of the shearing occurs in a fixed layer with hexagonal crystalline regions above and below the shear zone. This layered structure was typical of all high solids concentration calculations. The exact location of the shearing zone (or rolling layer) was not fixed and during a calculation it could shift up or down in the cell. The wide spread between the two calculated stress points on Figure 10 at a solids fraction of ν = 0.800 occurred because in one calculation (the lower point) a single rolling layer existed in exactly the same location for the entire calculation while in a subsequent calculation with a different set of initial random velocities (the upper point) the location of the shear zone kept shifting from one row to another. Each time a shift occurred temporary high-stress arches would form as the material "adjusted" from one configuration to the next. These temporary arches, while of short duration, had stresses large enough to
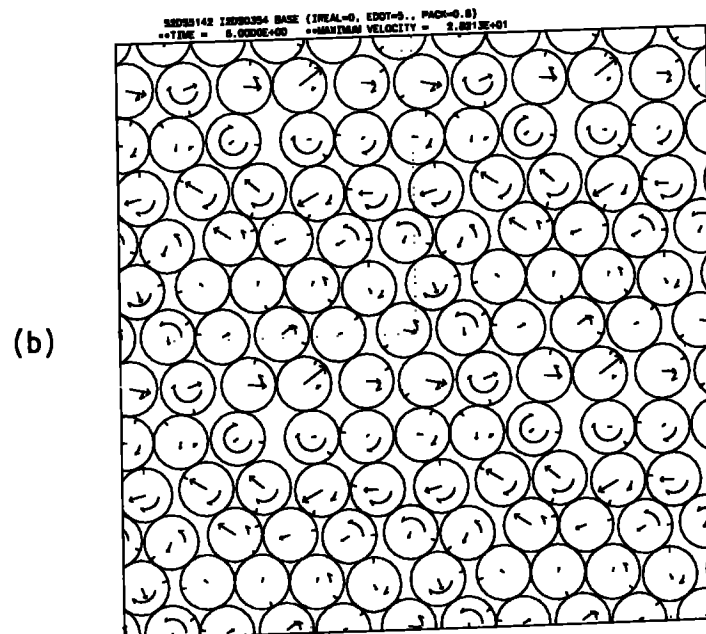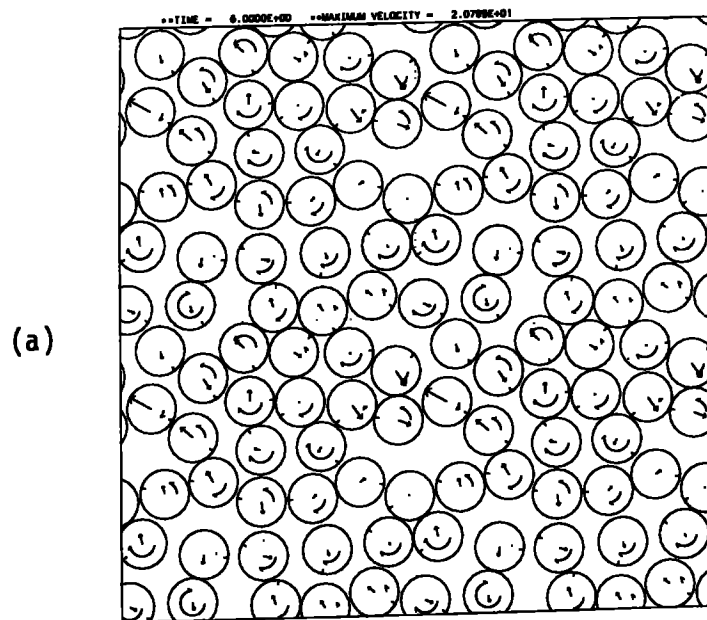
(a)

(b)

Figure 11. Primary calculational cell and 3 periodic image cells, each showing
the same 30 inelastic frictional particles during steady shearing
(a) with a solids fraction $v = 0.65$ and (b) with a solids
fraction $v = 0.80$. Deviatoric velocity vectors and rotational
velocities shown for each particle.

affect the cumulative time-averaged stress for the entire calculation. Because of the variable nature of these shearing simulations at densities above $\nu = 0.775$ they were only included in a limited number of cases.

The effect of interparticulate friction coefficient on the viscosity is shown in Figure 12. Three steady-state shearing calculation sets are shown. The partially filled circles are for frictionless particles (i.e., no rotations), the open circles are for a coefficient of friction $\mu = 0.5$ and the triangles are from Campbell and Gong's rigid body simulations[6] with $\beta = 0.0$, corresponding roughly to $\mu = \infty$. This plot shows that the inclusion of friction (and thus additional energy losses during glancing collisions) significantly reduces the shear stress at low packing fractions where the stress is primarily due to the momentum carried by the particles.

At high packing fractions, the inclusion of friction on the other hand, increases the shear stress significantly because the tangential forces acting during contacts are more effective at transmitting shear stress than normal forces acting alone. The pressure, $(p_{xx} + p_{yy})/2$, is also increased at high density when friction (and particle rotation) is included, although it is not increased by nearly as large a factor as the shear stress. The dimensionless shear stress results of Campbell and Gong's rigid body numerical calculations were scaled by multiplying by our effective particle material density, $\rho_p = 1/\pi$, and by the shear rate, $\dot\epsilon = 10$, to put them in the same units as the two-dimensional viscosity plotted in Figure 12. Their $\mu = \infty$ results are generally within 10% of our $\mu = 0.5$ values and, at least at low solids fractions, they are consistent with the notion that increasing the energy losses reduces the shear stress. The only point of significant disagreement appears at the highest solids fraction shown, $\nu = 0.78$, where there is a factor of two discrepancy between our curve and their reported value. It is quite possible that differences in friction,
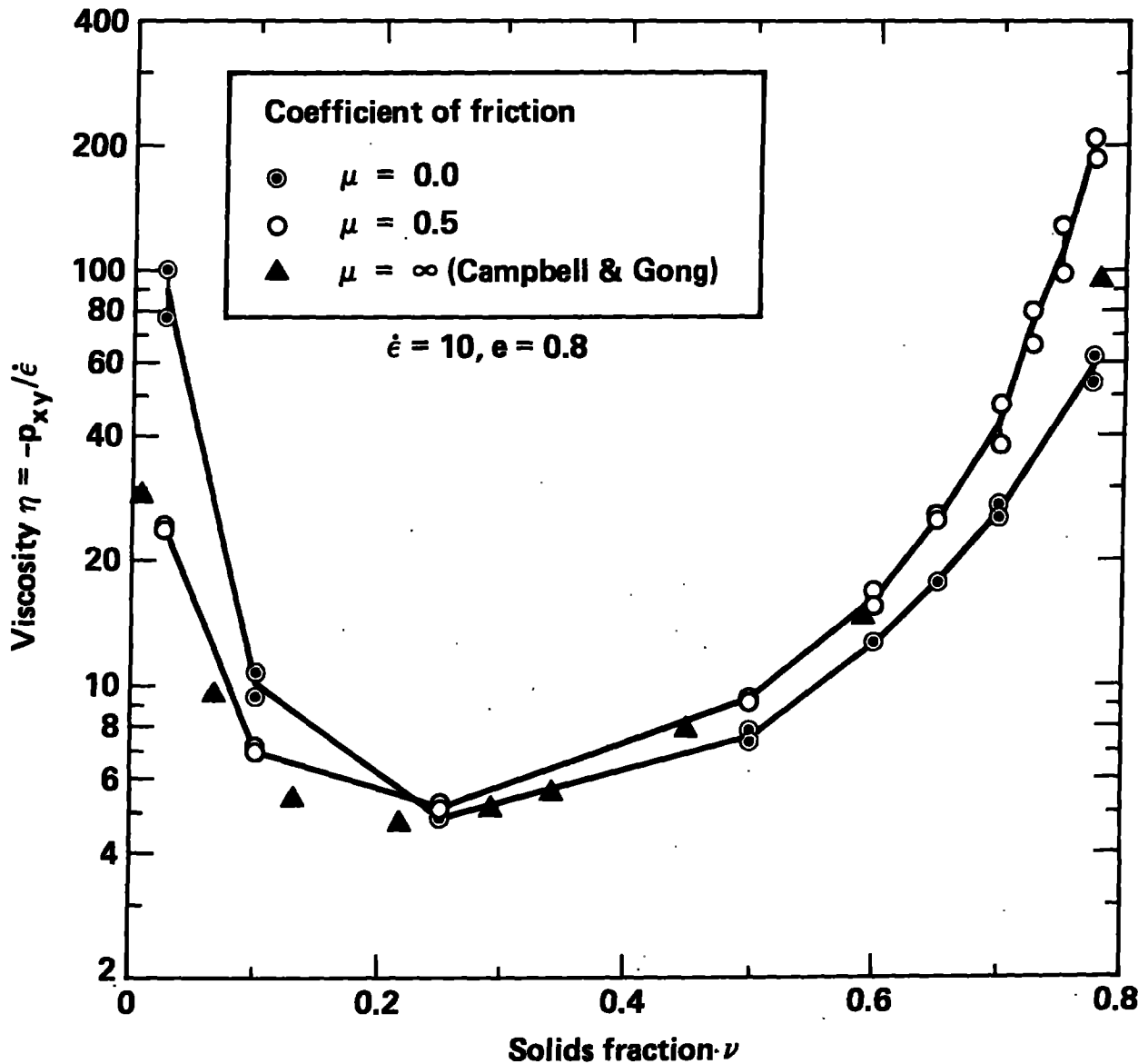
Figure 12. Calculated effective viscosity in steady shear flow with (μ = 0.50) and without friction (μ = 0.0) and as calculated by Campbell and Gong[6] with μ = ∞.

boundaries and sample size between our work and that of Campbell and Gong results in a layered shearing structure at a slightly lower packing fraction in their 80-particle planar boundary model than in our 30-particle periodic boundary model. Although not shown on Figure 12, our calculations at

ν = 0.800 gave viscosity values varying with time and ranging from 55 to 153, as the system shifted from one shear zone location to another, with an average value just over 100. This is within 10% of an extrapolation of Campbell and Gong's rigid body calculations.

These calculations are in contradiction with the three-dimensional rough particle theory of Lun and Savage[4] which predicts that the collisional part of the shear stress will be reduced by including frictional effects. Specifically for e = 0.8 they predict a reduction of collisional shear stress of approximately 20% in going from no friction (β = -1) to a very high friction (β = 0.0). Figure 12, shows on the other hand, a significant increase in the total shear stress when frictional interactions between particles are added. This increase is on the order of 50% at intermediate-to-high packing fractions where the stress tensor is dominated by collisional terms. Our total shear stress in this region, including frictional interactions, agrees with that of Campbell and Gong; however, since they do not report values for β = -1 (no friction) their calculations do not necessarily corroborate the increase in the collisional shear stress when friction effects are considered.

Figure 13, shows how varying the coefficient of restitution affects the calculated shear stress vs. solids fraction curve. All cases plotted on this figure have the same coefficient of friction μ = 0.500. As can be seen, changing the coefficient of restitution has the largest effect at low solids fractions where the stresses are primarily due to the momentum carried by the particles. Campbell and Gong report similar results and their calculations for e = 0.6 are about as close to the lower curve on this figure as their e = 0.8 calculations were to the μ = 0.5 line on Figure 12 (i.e., within about 10% except at the very lowest solids fractions). However, their e = 1.0 calculations give shear stresses that are significantly lower than our e = 1.0
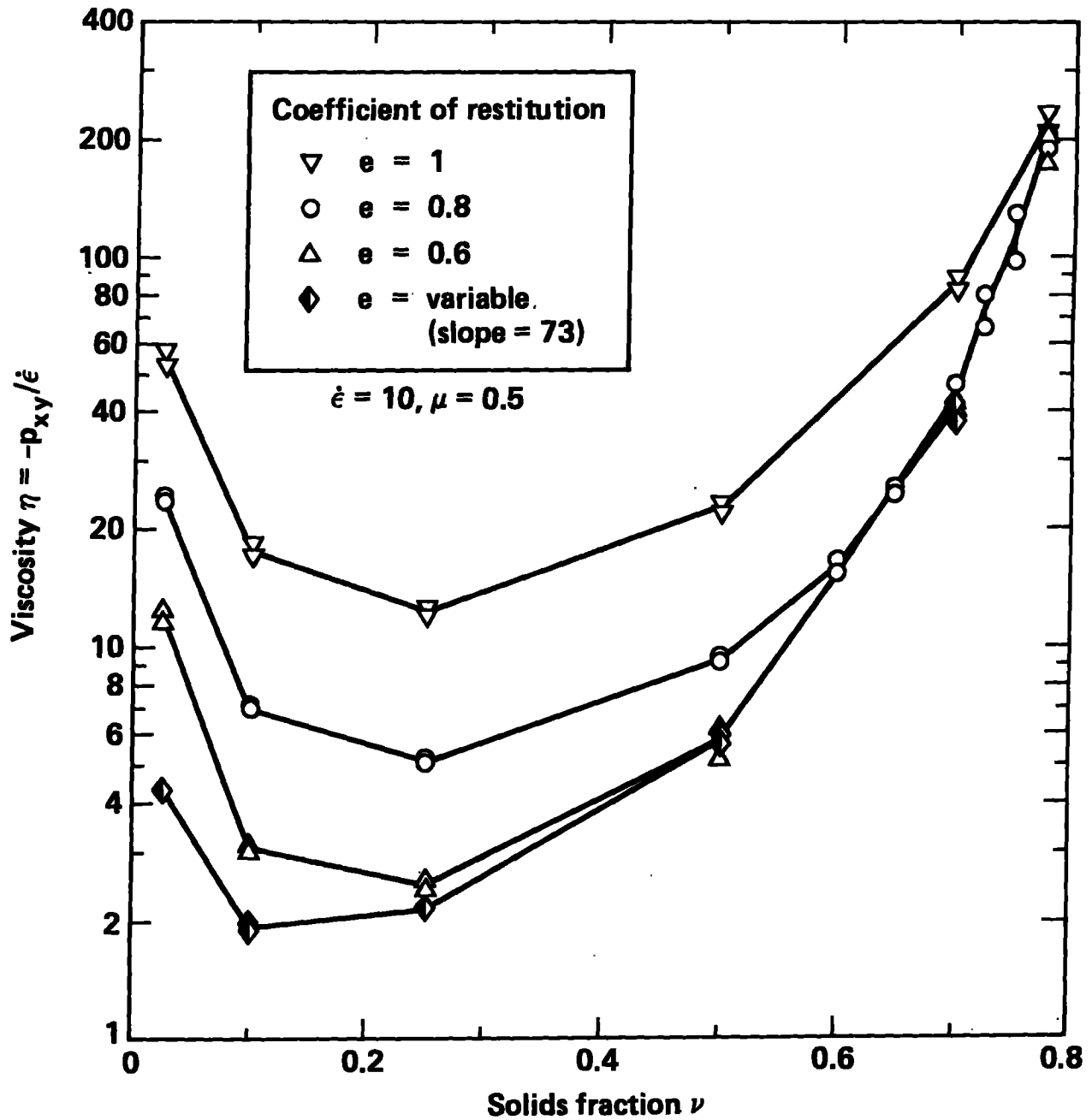
Figure 13. Calculated effective viscosity in steady shear flow using various coefficients of restitution.

curve at low solids fraction (with more than a factor of 2 difference at those low densities), but are essentially the same as our calculations at ν = 0.50. This discrepancy at low density is probably a direct consequence of the greater energy loss with their β = 0.0 collision operator than is produced with our μ = 0.5 friction model. The lower curve on Figure 13 shows the behavior we calculate with the variable coefficient of restitution model

(equations 5 and 6). This curve shows that as the packing fraction is reduced the higher mean deviatoric velocities cause the variable e material to behave like a material with a lower effective coefficient of restitution.

Stress and Velocity Distributions

Figure 14 shows the "dynamic friction coefficient", $\tan \phi_d = |p_{xy}|/p_{yy}$, as a function of solids packing fraction, ν. For frictionless particles the present two-dimensional calculations with e = 0.80, give a value of $\tan \phi_d \simeq 0.4$ over most of the density range, increasing to near 0.5 at extremely low packing. This is very close to the behavior predicted by Lun et al.[3] for three-dimensional frictionless particles with e = 0.80. Further, the addition of frictional interactions increases $\tan \phi_d$ to near 0.6 for intermediate solids fractions (.3 < ν <.65). This behavior is consistent with Lun and Savage's three-dimensional prediction[4] that strong frictional coupling will increase the dynamic friction coefficient from 0.40 to about 0.60 (as β changes from minus one to near zero) for a system with e = 0.80. The solid central curve on Figure 14 includes data from three different shearing rates to confirm that for material with a constant coefficient of restitution the dynamic friction coefficient is essentially independent of shear rate. This stress ratio does depend on the material properties and solids fraction as shown by the other curves on this figure. Campbell and Gong obtain similar curves for e = 1.0, 0.8, and 0.6; however, their calculations show a slightly steeper variation with solids fraction than the present work. In each of the three cases e = 1.0, 0.8, and 0.6, their calculations of $\tan \phi_d$ start 5% to 10% higher at low solids fractions, cross the curves of Figure 14 near ν = 0.3 and continue to decrease more rapidly than these curves as the solids fraction increases. At solids fractions near ν = 0.6 their calculated values are 10% to 30% lower than those of Figure 14.
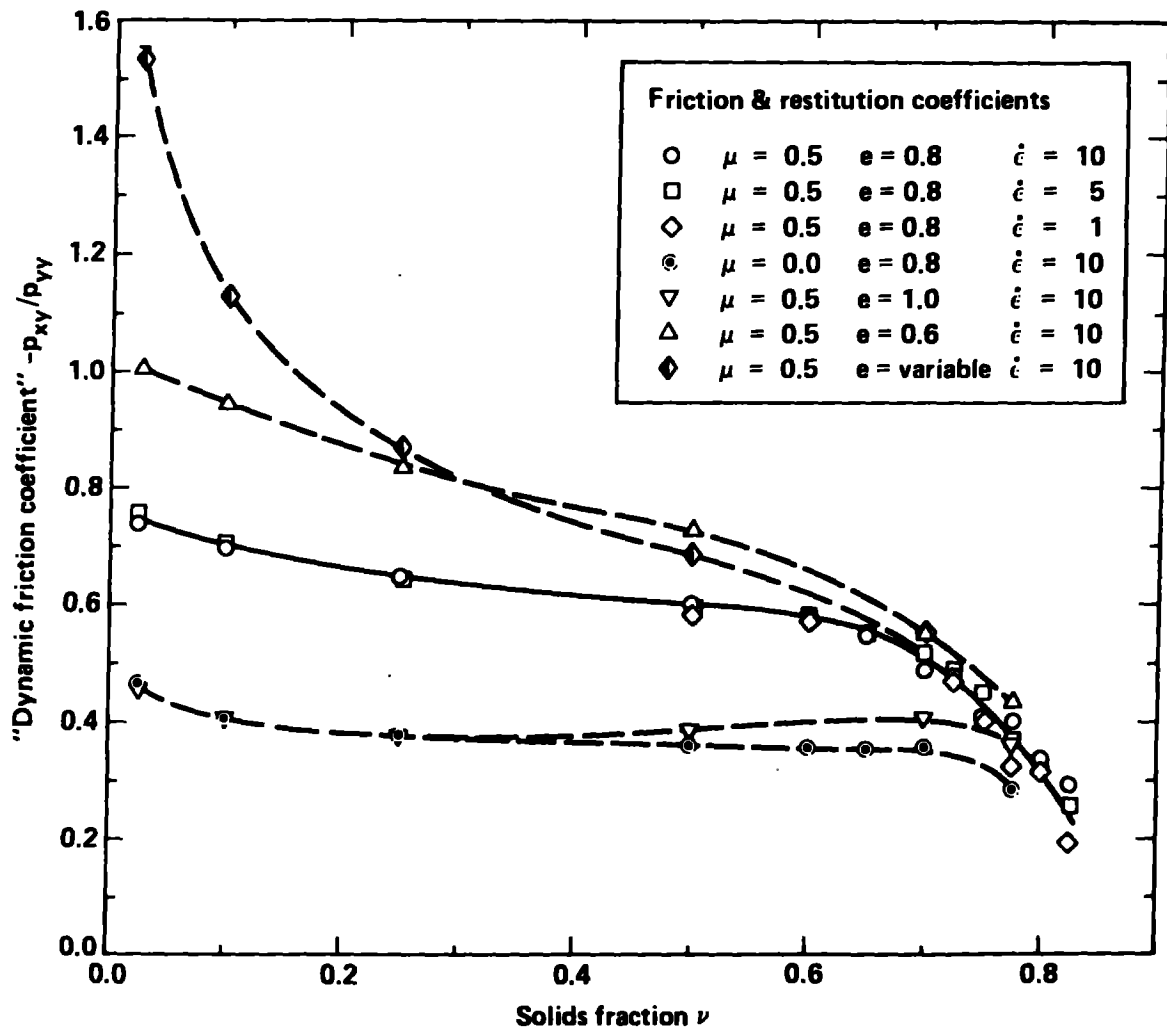
Figure 14. Calculated ratio of shear to normal stress components during steady shear for 30 inelastic, frictional disks at three shear rates (solid curve) and with various inelasticity and friction parameter values (dashed curves).

Laboratory maesurements of the dynamic friction coefficient for shearing systems of glass beads[27,28] and polystyrene beads[27] under rapid shearing conditions in annular shear cells produced dynamic friction coefficients in the range from 0.53 to 0.63 at densities near 80% of random close packing (a density which may correspond roughly to solids fractions in the range 0.65 to 0.70 for two-dimensional configurations). Since these materials have a coefficient of restitution between 0.8 and 0.95 we might

expect them to exhibit behavior that would lie between the e = 0.8 and e = 1.0 lines on Figure 14 . A value of tan ϕ_d greater than 0.53 is obtained in these calculations only for values of e at or below 0.80 in the density range 0.65 < ν < 0.70. This is just outside of the range of the experimental results; however, considering the difficulty in making any comparison between two-dimensional and three-dimensional systems, the proximity of these calculated two-dimensional values to the measured values is quite encouraging.

The variable restitution coefficient calculations produce a dynamic friction coefficient that diverges as ν approaches zero, an extension of the trend by the constant e calculations showing a higher value for tan ϕ_d for lower effective coefficients of restitution. This behavior can best be understood by examining the anisotropies in the stress and velocity distributions at these low solids concentrations.

Figure 15 shows the ratio of the two diagonal stress tensor components, p_{xx}/p_{yy}, where p_{yy} is the stress perpendicular to the shearing motion. The central solid curve in this figure, corresponding to e = 0.8, includes calculations at three different shearing rates, demonstrating again that the curves with e = constant are independent of shearing rate. At moderately high solids fraction (i.e., from ν = 0.4 to ν = 0.7), where the stress tensor is controlled by collisional terms we obtain an almost isotropic distribution of pressure. However, as the solids fraction decreases and/or the energy dissipation in the system increases we find the pressure distribution becoming more and more anisotropic. Each of the three curves e = 1.0, 0.8, and 0.6 given in this figure agree with corresponding rigid body calculations obtained by Campbell and Gong[6] (using β = 0.0) in the solids fraction range 0.1 < ν < 0.60. This anisotropy in the pressure distribution occurs because at low solids concentrations the deviatoric velocities are also very anisotropic. At low densities the mean free path for a particle is quite long
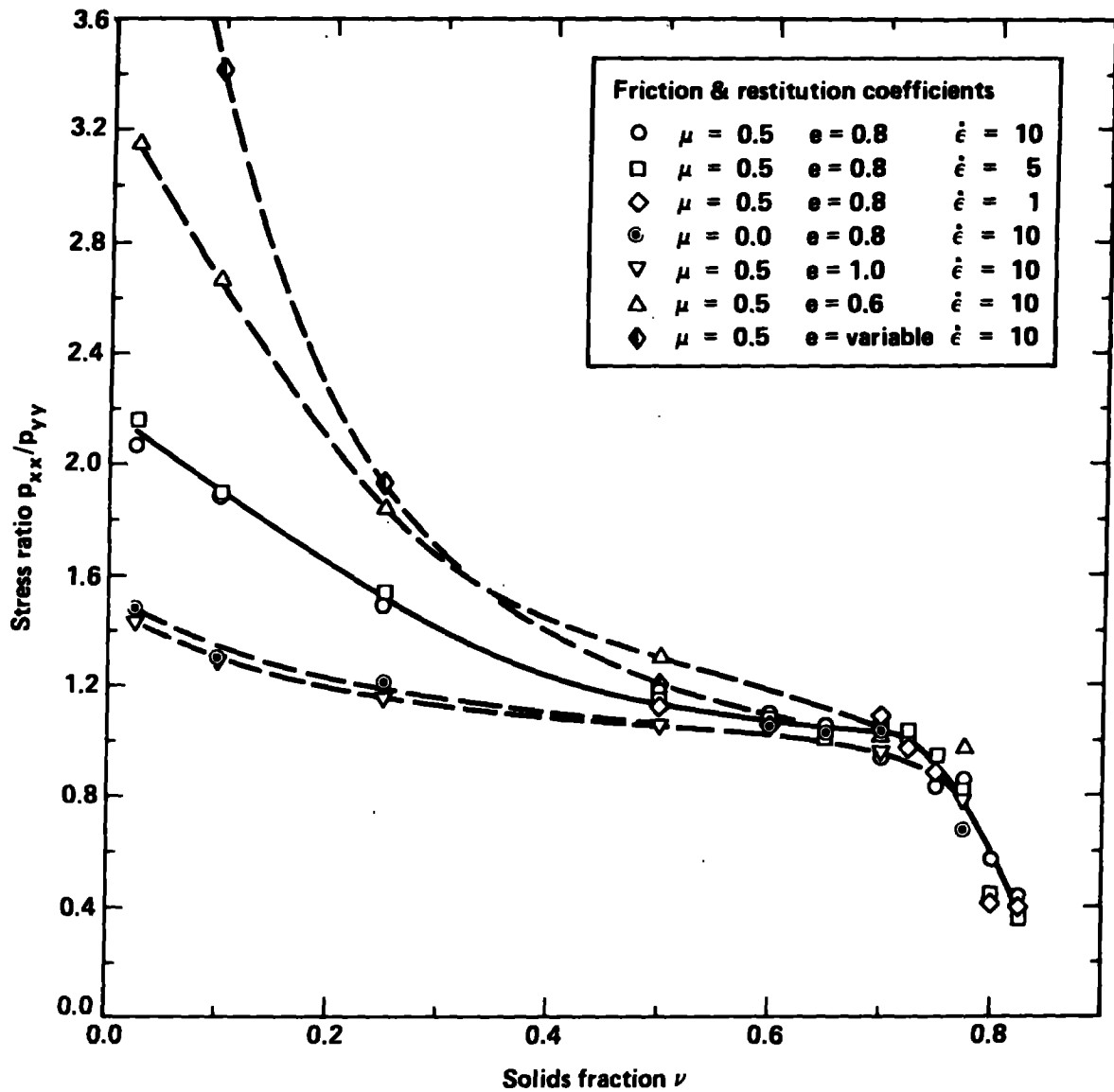
Figure 15. Calculated ratio of horizontal to vertical stress tensor components
during steady shearing in the x-direction, for 30 inelastic,
frictional disks showing anisotropic distribution at low solids
concentrations.

and it is possible for a particle to travel vertically through the system a

significant number of particle diameters before encountering another

particle. The more vertical distance traveled along a straight line

(collision free) trajectory the greater the deviatoric velocity of the

particle is likely to become (since the x-velocity of the particle remains

constant, but the "mean field velocity", u_x, changes linearly with vertical

position). Thus, when collisions do occur in these low concentration systems they are much more likely to have a large relative x-velocity than a large y-velocity. In a perfectly elastic system the random nature of collision interactions would soon produce an equi-partition of kinetic energy in the x- and y-directions; however, in the dissipative collisions of these calculations the kinetic energy gets dissipated before a sufficient number of collisions occur for it to become distributed isotropically. The anisotropic shearing deformation continues to feed kinetic energy into the x-direction by virture of the long mean free paths between collisions at low solids concentrations so that the net result is an anisotropic velocity distribution. Figure 16a shows the time-averaged distribution of velocities in the x, y, and θ directions in a representative calculation with $\mu = 0.5$, $e = 0.8$, and $\dot{\epsilon} = 10$ at a solids fraction of $\nu = 0.65$. The x- and y-velocities in this figure are distributed almost identically about zero, while the mean particle rotation is displaced somewhat from zero. Figure 16b shows the same velocity distributions for a lower solids concentration ($\nu = 0.1$) and with more dissipative interactions ($e = 0.6$, $\mu = 0.5$). In this figure the deviatoric x-velocity distribution is significantly different from the y-velocity distribution. It should be noted that the p_{xx} stress component exceeded the p_{yy} component in the calculation corresponding to Figure 16b by a factor of more than 2.5.

Another stress ratio examined is the ratio of the shear stress to the pressure, $2|p_{xy}|/(p_{xx} + p_{yy})$. This quantity is plotted in Figure 17 and, as can be seen, is much less dependent on the solids concentration than the dynamic friction coefficient of Figure 15. It does still show a consistent variation with particle interaction parameters μ and e.
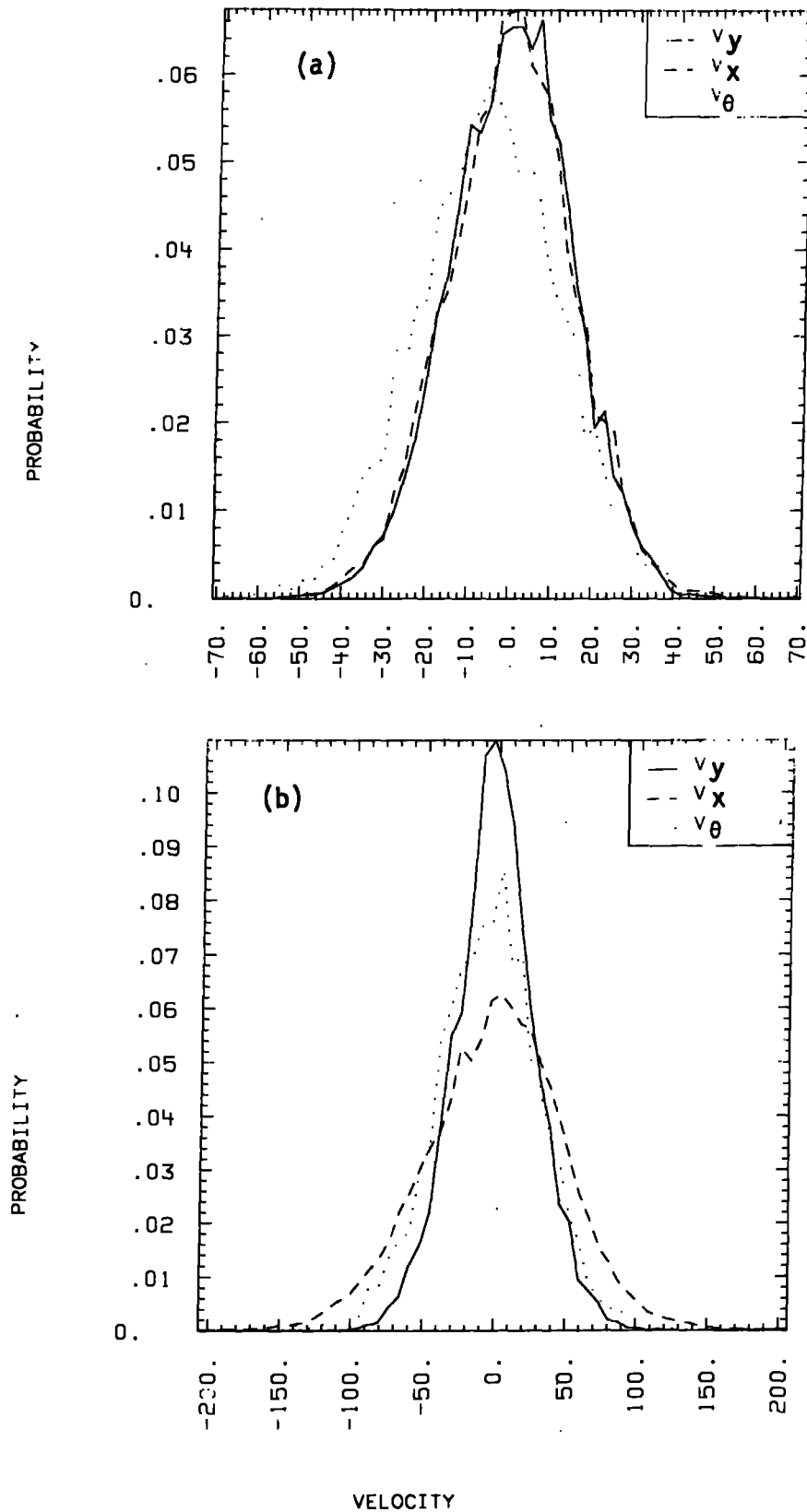
Figure 16. Cumulative time average of velocity probability distributions in the x, y, and Θ directions for a set of 30 particles in steady shear with (a) solid fraction ν = 0.65 with e = 0.8, μ = 0.50, and (b) solids fraction ν = 0.10, e = 0.6, μ = 0.50.
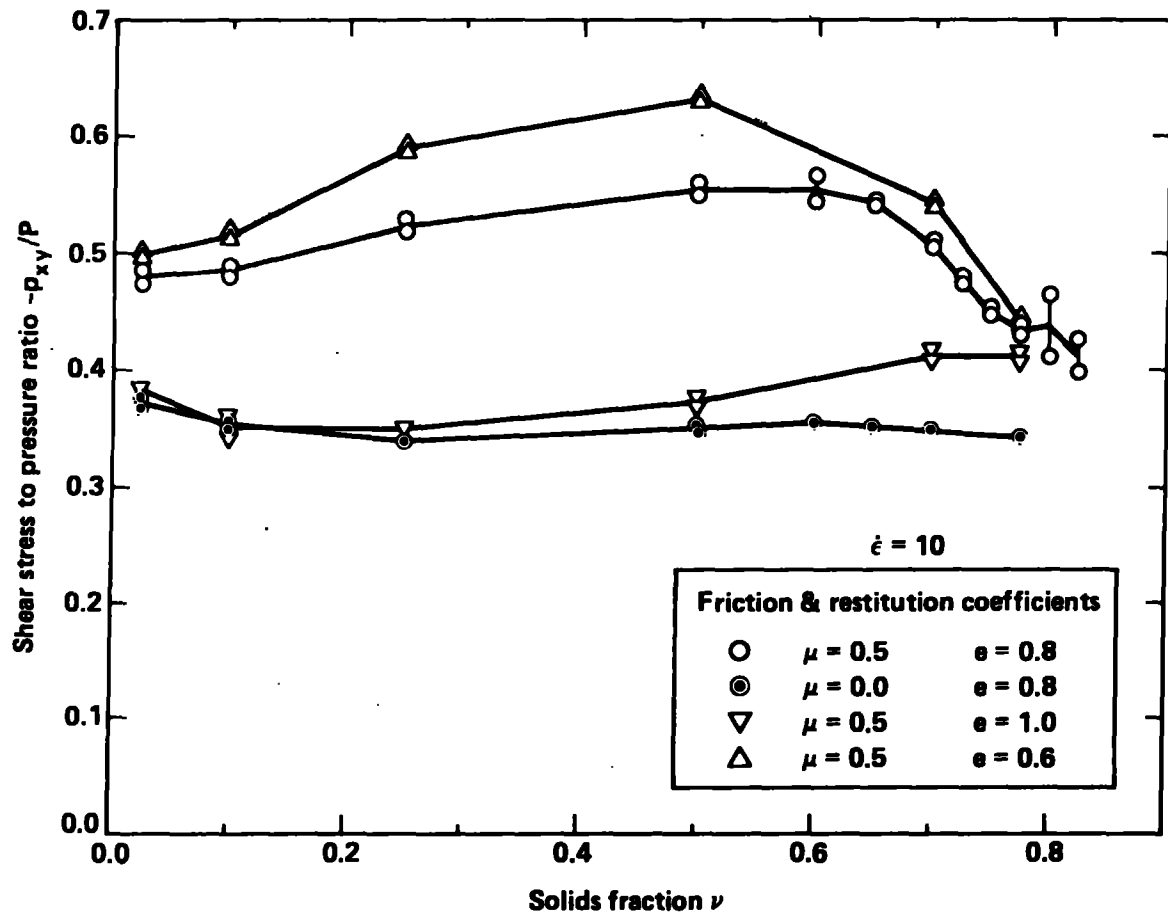
Figure 17. Calculated ratio of shear stress to total pressure during steady shear for 30 inelastic, frictional disks.

The velocity distributions of Figure 16 included the distribution of rotational velocities with a clearly non-zero mean value. In all shearing calculations involving frictional particles we found the mean rotational velocity was nearly equal to one half the shear rate, $\dot{\epsilon}/2$. Figure 18 shows the cumulative average spin values obtained in over 50 separate calculations. In every case the mean spin is near $\dot{\epsilon}/2$. At very low solids concentrations the calculations deviate from this behavior, but at these concentrations the rotational velocity distribution is very broad and our calculations of mean rotational velocity are of low accuracy. These low solids concentration calculations took considerably more computer time than calculations at higher
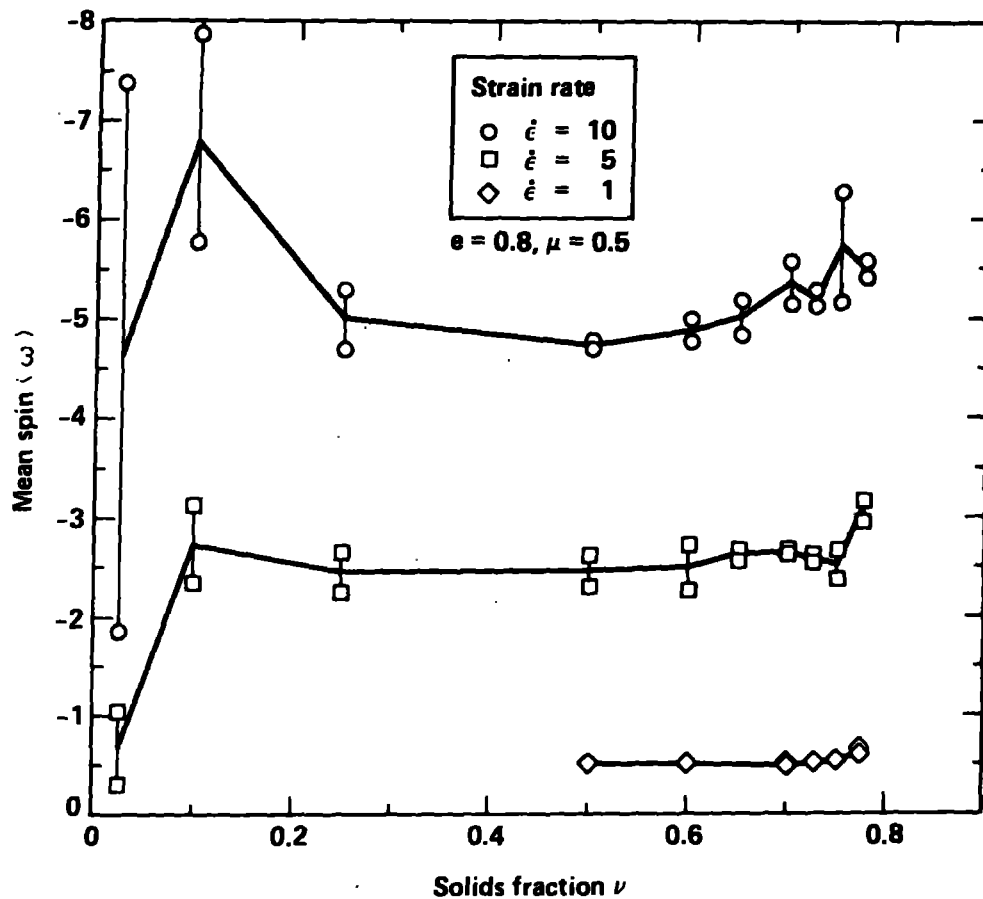
Figure 18. Calculated mean rotational velocity for disks in a 30-particle
system undergoing steady shear at various strain rates showing mean
spin nearly equal to one-half the strain rate.

densities so they have not been repeated to improve the accuracy of the low

concentration spins. These rotational velocity results are consistent with

other researchers' calculations both for frictional particles[6] and for

asymmetric elastic particles[14].

CONCLUDING REMARKS

A non-equilibrium molecular-dynamics-like calculational technique has been

employed to examine the effects of inelasticity and friction on shearing two-

dimensional assemblies of disks. This simulation of granular flow deals with

a very simple system of equal-sized symmetric particles, yet it provides a

great deal of insight into the mechanisms that cause the observed behavior

(e.g., the anisotropy in the pressure and velocity distributions at low density). Much of the two-dimensional granular flow behavior calculated in this study is in qualitative agreement with recent microstructural theories developed for three-dimensional systems. However some of the features were not expected, such as the increases in the collisional contribution to the stress tensor components at moderately high densities when frictional effects are included.

Qualitative comparisons between two-dimensional computer simulations of granular flow and physical tests with particles restricted to two-dimensional motion have shown very great similarity[8,29]; however, almost no quantitative comparisons have been performed. This is partially because few experimental studies on two-dimensional systems have included measurements of stress, deviatoric velocity and density distributions. Likewise, few calculational models can handle the three-dimensional particles that are used in most laboratory tests. This situation will soon change. At least two independent studies are underway that will provide detailed particle trajectory, velocity and density distribution measurements for gravity flow on inclines[30] and vertical channel and rectilinear shear flow[31] of two-dimensional systems. When data from these experiments are available it will be possible to make quantitative comparisons between calculations like the present study and measurements on comprable systems. Likewise, as the capabilities of the computer models are improved to include various three-dimensional configurations it will be possible to perform direct computer simulations of many of the existing laboratory studies on granular systems. We anticipate that such comparisons will be possible within the next year or two.

Acknowledgments

References

1. Jenkins, J. T. and Savage, S. B., "A Theory for the Rapid Flow of Identical, Smooth, Nearly Elastic, Spherical Particles", J. Fluid Mech. Vol. 130, 1983, pp. 187-202.

2. Haff, P. K., "Grain Flow as a Fluid Mechanical Phenomenon", J. Fluid Mech., Vol. 134, 1983, pp. 401-430.

3. Lun, C. K. K., Savage, S. B., Jeffrey, D. J., and Chepurniy, N., "Kinetic Theories for Granular Flow: Inelastic Particles in Couette Flow and Slightly Inelastic Particles in a General Flow Field", J. Fluid Mech. Vol. 140, 1984, pp. 223-256.

4. Lun, C. K. K. and Savage, S. B., "A Simple Kinetic Theory for Granular Flow of Rough, Inelastic, Spherical Particles", J. Appl. Mech. (to appear).

5. Ackerman, N. L. and Shen, H. "Stresses in Rapidly Sheared Fluid-Solid Mixtures", J. of Engng. Mech. Div. A.S.C.E., Vol. 108, 1982, pp. 95-113.

6. Campbell, C. S. and Gong, A., "The Stress Tensor in a Two-Dimensional Granular Shear Flow", J. Fluid Mech. (to appear).

7. Campbell, C.S. and Brennen, L. E, "Computer Simulation of Granular Shear Flows", J. Fluid Mech. Vol. 151, 1985, p. 167.

8. Walton, O. R., "Particle Dynamics Calculations of Shear Flow", in Mechanics of Granular Material: New Models and Constitutive Relations, J. T. Jenkins and M. Satake, Eds., Elsevier Sci. Pub., Amsterdam, Netherlands, 1983, pp.327-338.

9. Cundall, P. A. and Strack, O. D. L., "A Discrete Numerical Model for Granular Assemblies", Geotechnique, March 1979.

10. Cundall, P. A. and Strack, O. D. L. "The Distinct Element Method as a Tool for Research in Granular Media", Report to NSF on Grant ENG-76-20711, Univ. of Minnesota Report, Oct. 1979.

11. Hoover, W. G., "Rheology via Non-equilibrium Molecular Dynamics" presented at Soc. of Rheology Mtg., October 1982.

12. Hoover, W. G. and Ashurst, W. T., "Non-equilibrium Molecular Dynamics", Adv. in Theo. Chem., 1, 1975, pp. 1-51

13. Evans, D. J., "The Non-Symmetric Pressure Tensor in Polyatomic Fluids", J. Stat. Phys., Vol. 20, No. 5, 1979, p. 547.

14. Evans, D. J., "Non-Equilibrium Molecular Dynamics Study of the Rheological Properties of Diatomic Liquids", Mol. Phys., Vol. 42, No. 6, 1981, pp. 1355-1365.

15. Walton, O. R., Hagen, D. A., and Cooper, J. M. "Interparticulate Force Models for Computational Simulation of Granular Solids Flow", presented at XVIth It'l Cong. of The. & Appl. Mech. Aug. 19-25, 1984, Lyngby, Denmark; also: Walton, O. R., Brandeis, J., Cooper, J. M., "Modeling of Inelastic, Frictional, Contact Forces in Flowing Granular Assemblies" presented at 21st Soc. Engng. Sci. Mtg., Blacksburg, VA Oct. 1984 (In preparation)

16. Hallquist, J. O., DYNA2D- An Explicit Finite Element and Finite Difference Code for Axisymmetric and Plane Strain Calculations, (Users Guide), Lawrence Livermore National Laboratory Rept., UCRL-52429, 1978.

17. Timoshenko, S. and Goodier, J. N., Theory of Elasticity, 2nd edition, McGraw Hill, NY, 1951.

18. Goldsmith, W. Impact, Edward Arnold Pub., London, 1960.

19. Hallquist, J. O., NIKE2D- A Vectorized, Implicit Finite-Deformation, Finite Element Code for Analyzing The Static and Dynamic Response of 2-D Solids, Lawrence Livermore National Laboratory Rept. UCID-19677, Feb. 1983.

20. Mindlin, R. D., "Compliance of Elastic Bodies in Contact", J. Appl. Mech. Trans. ASME, Vol. 16, 1949, pp. 259-268.

21. Mindlin, R. D. and Deresiewicz, H., "Elastic Spheres in Contact Under Varying Oblique Forces", J. Appl. Mech., Trans ASME Vol. 20, 1953, pp. 327-344.

22. Oden, J. J. and Martins, J. A. C., "Models and Computational Methods for Dynamic Friction Phenomena", proceedings FENOMECH III, Stuttgart, W. Germany, Computer Methods in Appl. Mech. and Engng., North Holland, Amsterdam, 1984.

23. Hoover, W. G. and Alder, B. J., "Studies in Molecular Dynamics, IV. The Pressure, Collision Rate, and Their Number Dependence for Hard Disks", J. Chem. Phys., Vol. 46, No. 2, 1967, pp. 686-691.

24. Evans, D. J., "Non-Linear Viscous Flow in Two-Dimensional Systems", Phys. Rev. A. Vol. 22, No. 1, 1980, pp. 290-294.

25. Bagnold, R. A., "Experiments on a Gravity Free Dispersion of Large Solid Spheres in a Newtonian Fluid Under Shear". Proc. R. Soc. Lond. A, 225, 1954, pp. 49-63.

26. Hopkins, M. A., "Collisional Stresses in a Rapidly Deforming Granular Flow", M.S. Thesis, Clarkson University, Potsdam, N.Y. April 1985, and Shen, H. (private communication) 1985.

27. Savage, S. B. and Sayed M., "Stresses Developed by Dry Cohesionless Granular Materials Sheared in an Annular Shear Cell", J. Fluid Mech. (1984) Vol. 142, pp 391-430.

28. Hanes, D. M. and Inman, D. L., "Observations of Rapidly Flowing Granular-Fluid Materials", J. Fliud Mech. (1985) Vol. 150, pp357-380.

29. Walton, O. R. "Explicit Particle Dynamics Model for Granular Materials", Numerical Methods in Geomechanics Edmonton 1982, Vol. 3, pp1261-1268, edited by Z. Eisenstein, A.A. Balkema, Rotterdam.

30. Drake, T. G. and Shreve, R. L., "High-speed Motion Pictures of Steady, Parallel Two-Dimensional Inertial Flows of Granular Materials", presented at 56th Soc. of Rheology Mtg. 25-27 Feb. 1985, Blacksburg, VA (also, private communication, 1985).

31. Shen, H. and Ackerman, N. (private communication, 1985) Clarkson University, Potsdam, N.Y.